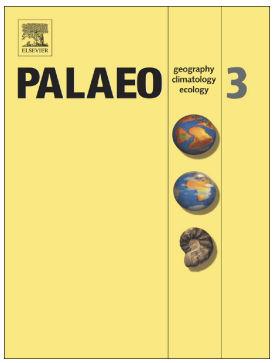

Sedimentary geochemistry of Late Cretaceous-Paleocene deposits at the southwestern margin of the Anambra Basin (Nigeria): Implications for paleoenvironmental reconstructions

Erepamo J. Omietimi, Nils Lenhardt, Renchao Yang, Annette E. Götz, Adam J. Bumby

PII: S0031-0182(22)00229-2

DOI: https://doi.org/10.1016/j.palaeo.2022.111059

Reference: PALAEO 111059

To appear in: *Palaeogeography, Palaeoclimatology, Palaeoecology*

Received date: 1 December 2021

Revised date: 11 May 2022

Accepted date: 15 May 2022

Please cite this article as: E.J. Omietimi, N. Lenhardt, R. Yang, et al., Sedimentary geochemistry of Late Cretaceous-Paleocene deposits at the southwestern margin of the Anambra Basin (Nigeria): Implications for paleoenvironmental reconstructions, *Palaeogeography, Palaeoclimatology, Palaeoecology* (2021), https://doi.org/10.1016/j.palaeo.2022.111059

Sedimentary geochemistry of Late Cretaceous-Paleocene deposits at the southwestern margin of the Anambra Basin (Nigeria): Implications for paleoenvironmental reconstructions

Erepamo J. Omietimi[a], Nils Lenhardt[a,*], Renchao Yang[b,c,**], Annette E. Götz[d], Adam J. Bumby[a]

[a]Department of Geology, University of Pretoria, Private Bag X20, 0028 Pretoria, South Africa

[b]College of Earth Science and Engineering, Shandong University of Science and Technology, Qingdao 266590, Shandong, China

[c]Laboratory for Marine Mineral Resources, Qingdao National Laboratory for Marine Science and Technology, Qingdao 266071, Shandong, China

[d]Department of Structural Geology and Geodynamics, Georg-August-University Göttingen, 37077 Göttingen, Germany

[*]Corresponding author: Department of Geology,
University of Pretoria,
Private Bag X20
0028 Pretoria
Republic of South Africa
E-Mail: nils.lenhardt@up.ac.za

** also corresponding author: e-mail: yang100808@126.com

Abstract

The Campano-Maastrichtian deposits of the Nkporo and Mamu formations of the Anambra Basin represent prospective hydrocarbon resources in southern Nigeria. In order to reveal the paleoclimate, sediment recycling and paleoenvironment during the deposition of these formations in the southwestern portion of the Anambra Basin, a detailed geochemical analysis was performed using major elements, trace elements and rare earth element data, as well as the mineralogical characterization of 20 samples from two wells. The combination of geochemical ratios (Rb/Sr, Th/U, and C-value) and weathering indices (CIA, CIW, and PIA) demonstrates that the region experienced a warm, humid tropical paleoclimate throughout the Late Cretaceous. Furthermore, West Africa experienced strong precipitation during the Cretaceous, leading to intense chemical weathering in the region, as documented by the geochemically matured sediments.

The paleosalinity (Sr/Ba) and paleoproductivity (Ba/Al and P/Ti) proxies show that the studied mudrocks were deposited primarily in brackish to shallow-marine settings, with poor primary productivity due to terrestrial clastic influx and hydrodynamic influence. Using multiple paleoredox indicators, deposition under oxic conditions is detected. The low authigenic U enrichment and depleted V and Cr values normalized to UCC standards further support oxic bottom water conditions. Wavy laminations observed in the mudrocks indicate retreating seawater and high hydrodynamic conditions. Ultimately, the southwestern Anambra Basin reveals Late Cretaceous-Paleocene deposits of a shallow sea controlled by a strong hydrodynamic regime.

Keywords: Late Cretaceous; Shale lithofacies; Sediment geochemistry; paleoenvironment proxy; paleoclimate proxy; paleotemperature proxy; depositional conditions

1. Introduction

During the last three decades, research in sedimentary geochemistry of siliciclastic deposits progressed significantly (Nath et al., 1997; Barbera et al., 2006; Elliot et al., 2009; Fu et al., 2016; Zhang et al., 2020), and it is now used to decipher - among other factors - paleoclimatic and paleoenvironmental conditions, sediment recycling, biogenic silica inputs, hydrothermal influence, and paleo-hydrodynamic force (Jones and Manning, 1994; Barbera et al., 2006; Martinez-Ruiz et al., 2015; Fu et al., 2016; Li et al., 2018a; Wei and Algeo, 2020; Wei et al., 2021). The chemical composition of sedimentary rocks is strongly influenced by factors such as the chemical constituents of the source area, the energy of the transport medium and the increasing distance away from the source, marine and freshwater incursions, the water depth, the existence or absence of hydrothermal fluids, and the climatic, weathering and redox conditions during sedimentation (Moradi et al., 2016). These factors leave their imprint in the resulting deposits that can be deciphered by analyzing their unique geochemical signature (Li et al., 2018b; Pehlivanli, 2019). Major elements (Al, Fe, Mn, and Ti), high field strength elements (U, Th, and Zr), large ion lithophile elements (Sr, Ba, and Rb), and transition elements (Co, Zn, Cr, V, Ni, and Cu) are all transported to the sedimentary basin without substantial fractionation and thereby retain the signature of the depositional environment (Tribovillard et al., 2006; Kahmann et al., 2008; Moradi et al., 2016). Furthermore, immobile (Zr, Fe, Al, Th) and mobile (Sr, Ba, Rb) chemical elements can be used to assess the paleoclimate, paleoredox and hydrothermal conditions and the hydrodynamic pressure during sedimentation (Rimmer, 2004; Zhong et al., 2015; Goldberg and Humayun, 2016; Moradi et al., 2016; Tao et al., 2017; Li et al., 2018b; Pehlivanli, 2019; You et al., 2020). These geochemical proxies are therefore of immense

importance for the reconstruction of the changing environmental conditions during sedimentation in a (petroliferous) basin, which c make them an important tool for petroleum geologists. The Late Cretaceous and Paleocene epochs experienced extreme global temperature conditions (Hay and Floegel, 2012; Scotese et al., 2021). In West Africa, warm temperature conditions typical of tropical climates were recorded in the geologic record (Chumakov et al., 1995; Scotese et al., 2021).

The Anambra Basin (Fig. 1), which is younger than the lower part of the Benue Trough, is a Cretaceous-Paleogene hydrocarbon-rich sedimentary basin in Nigeria, West Africa, with mainly gas prone hydrocarbon potential (Ene et al., 2019). Over the last two decades, several studies focusing on sedimentology (Tijani et al., 2010; Onyekuru and Iwuagwu, 2010; Dim et al., 2019) and stratigraphy (Uzoegbu et al., 2013), mineralogy (Akinyemi et al., 2013), palynology (Antolinez-Delgado and Oboh-Ikuenobe, 2007), reservoir characterization (Anakwuba and Onyekwelu, 2010; Okwara et al., 2020), petroleum potential (Akaegbobi et al., 2000; Adebayo et al., 2018; Ogungbesan and Adedosu, 2020), aeromagnetics (Onwuemesi, 1997; Bello et al., 2017), and gravity modelling (Obasi et al., 2018; Omietimi et al., 2021) have been carried out on the basin. Most of the research focuses on the basin's center and eastern margin (Tijani et al., 2010; Edegbai et al., 2019a). In contrast, little research has been carried out on its western margin (Ocheli et al., 2018; Edegbai et al., 2020; Ogungbesan and Adedosu, 2020).

The Imo, Mamu and Nkporo formations (Fig. 2) are thought to have been deposited within estuarine, marginal to shallow-marine environments in a passive tectonic setting with their sediments largely derived from continental granitic rocks (Odunze and Obi, 2011; Odunze et al., 2013; Edegbai et al., 2019a). Nevertheless, there is still a plethora of open questions and a variety of unknown factors, particularly concerning the paleogeographic redox conditions,

paleowater depth, hydrothermal influence, and paleohydrodynamic regime during deposition. The present study utilized drill core and ditch cuttings to provide a robust dataset compared with existing data on outcrop samples that are prone to alteration. Here, we use sedimentary geochemistry to constrain these parameters and reveal the major controlling factors during sedimentation. These findings will provide a better understanding of the sedimentation within the southwestern part of the basin. This study will also provide useful information for future research on siliciclastic systems, both locally and globally, as it takes a systematic approach to determine paleoredox conditions during deposition, hydrothermal impact, hydrodynamic strain, and ancient water depth using the example of the Late Cretaceous and Paleocene Nkporo, Mamu and Imo formations.

2. Geological setting

2.1. Regional and tectonic setting

Nigeria's Anambra Basin is part of the West and Central African Rift System (WCARS) basins (Abubakar, 2014) that started to form during the Early Cretaceous when Gondwana began to break apart and the South Atlantic Ocean started to open (Burke and Whiteman, 1973; Fairhead, 1988; Benkhelil, 1989). The basin formed during the post-deformational sedimentation period during the evolution of the Benue Trough, followed by Santonian inversion tectonics across the basin (Obaje, 2009; Mode et al., 2016; Edegbai et al., 2019a).

The Anambra Basin is one of seven sedimentary basins in Nigeria (Fig. 1), featuring a structural depression at the southwestern margin of the Lower Benue Trough. It covers an area of ca. 40,000 km^2 and stretches across Nigeria's Anambra, Enugu, and Ebonyi states, and extends southwards to part of Delta state, northwards into Benue and Kogi states, and westwards to the

Edo province (Akaegbobi et al., 2000; Edegbai et al., 2019a). Geological, well/core data, gravity, magnetic and seismic modelling have shown that the Anambra Basin contains a >6 km thick sedimentary succession, representing a sequence of continental, deltaic, and marginal marine sedimentation (Agagu and Adighije, 1983; Obasi et al., 2018; Dim et al., 2019; Omietimi et al., 2021). The oldest sediments within the basin date from the Campanian age, and deposition continued through the Late Cretaceous into the early Paleogene.

2.2. Stratigraphy

The Anambra Basin comprises Campanian, Maastrichtian, and Paleocene sediments (Fig. 2). The basin subsided during the Santonian period, which accompanied the main tectonic process, and an E-W prograding deltaic system formed, with the Campanian marine Nkporo and Enugu formations being the first to be deposited comprising mainly marine dark grey shales, sandy shales, sandstones, and ironstones (Akande and Mücke, 1993; Akaegbobi et al., 2000). Maastrichtian deposits of the Mamu Formation comprise shales, sandstones, siltstones, clays, sandy shales, shaly sands, clayey shales, ironstones, and coal seams of fluvio-deltaic to marginal marine depositional environments (Dim et al., 2019; Edegbai et al., 2019a). The overlying Ajali Formation was deposited in a shallow marine to terrestrial environment (Tijani et al., 2010), and its thickness varies across the basin. The Nsukka Formation, conformably overlying the Ajali Formation, marks the termination of Maastrichtian deposits and the onset of Paleocene sedimentation. The formation accumulated in bay, mud flat, lagoonal, shoreface and shallow-marine environments during a period of transgression (Mode and Odumodu, 2015) and is more developed in the basin's eastern portion, where complete sections are available; in the western part, it is only represented by a thin unit that caps the Ajali Formation

(Edegbai et al., 2019a). In the late Paleocene, the Imo Formation was deposited, characterized by foreshore and shoreface to delta front deposits (Oboh-Ikuenobe et al., 2005). This formation is considered the subsurface equivalent of the Akata Formation in the Niger Delta Basin (Reijers et al., 1997; Odunze and Obi, 2011; Adeleye and Daramola, 2018).

- place **Figure 1** near here -

2.3. Sedimentary environment

The Nkporo, Mamu and Imo formations are characterized by dark-grey shales and claystones and an alternation of siltstones, sandstones and coal seams (Ola-Buraimo et al., 2016; Edegbai and Schwark, 2020). These lithofacies have been intersected by the studied Owan-1 and Ubiaja wells (Figs. 3 and 5). The Ajali and Nsukka formations probably thinned out and were not intersected within the studied wells in the western part of the basin (original report from oil companies). In the eastern part of the basin, the lithofacies of the Nkporo Formation represents marine and inner estuarine environments (Odunze et al., 2013). The Mamu Formation comprises brackish sediments at the basin's western margin, while the central basin features marsh and bay depositional environments (Edegbai et al., 2019a). In contrast, Dim et al. (2019) classified the Mamu Formation's lithofacies at the basin's eastern margin into lagoonal, barrier island, shoreface, offshore transition zone and open shelf depositional environments. In the lower Benue Trough, Odunze et al. (2011) classified the lithofacies of the Imo Formation into tidal, estuarine, and marine facies. These authors further described high-frequency regressive and transgressive sequences in lagoonal coastal swampy settings to shelf depositional settings.

- place **Figure 2** near here -

3. Materials and methods

Two drill cores, the Owan-1 and the Ubiaja wells that are stored and curated by the Nigerian Geological Survey Agency in Kaduna were studied. Both wells were drilled in the western segment of the Anambra Basin and reached a depth of 600 m and 970 m, respectively (Figs. 3 and 5), intersecting the Late Cretaceous Mamu, Nkporo and Paleocene Imo formations. The main lithofacies types (see section 3.1) were sampled in regular intervals for geochemical analyses.

Twenty (20) samples were used for geochemical analysis (electronic supplementary material 1). Circa 7-10 g of each sample were crushed to <75 µm in a Tungsten Carbide milling vessel, roasted at 1000°C to determine Loss On Ignition (LOI), and fused into a glass bead. Major element oxides were determined on the fused bead by X-ray fluorescence (XRF) using an ARL9400XP + Wavelength dispersive XRF Spectrometer with Rh tube, LiF220, GER, AXO6 and PET analyzing crystals. Another aliquot of the sample was pressed into a powder briquette to determine trace elements. Preparation of samples and analyses were carried out using standard methods after Loubser and Verryn (2008).

Analyses of trace elements and REE were conducted at the Earth Lab of the University of the Witwatersrand using a Thermo Scientific iCAP RQ for inductively coupled plasma mass spectrometry (ICP-MS). X-ray diffraction (XRD) was carried out at the Stoneman Lab of the University of Pretoria, using a PANalytical X'Pert Pro powder diffractometer with X'Celerator detector and Fe filtered Co-K radiation.

For this study, the weathering and paleoclimate indicators CIA (Chemical Index of alteration; Nesbitt and Young, 1982), PIA (Plagioclase Index of Alteration; Fedo et al., 1995), CIW (Chemical Index of Weathering; Harnois, 1988) and C-value (Zhang et al., 2020) were computed and compared to PAAS (Post-Archean Australian Shale) and UCC (Upper Continental Crust) limits. The CIA, PIA, CIW and C-value are measured using the equations:

$$CIA=AL_2O_3/ (AL_2O_3+CaO^*+Na_2O+K_2O) \times 100 \quad (1)$$

$$PIA = [(Al_2O_3-K_2O)/ (Al_2O_3+CaO^*+Na_2O-K_2O)] \times 100 \quad (2)$$

$$CIW= [AL_2O_3/ (Al_2O_3+CaO^*+Na_2O)] \times 100 \quad (3)$$

$$C\text{-value} = [Fe + Mn + Cr + Ni + V + Co]/ [Ca + Mg + Sr + Ba + K + Na] \quad (4)$$

where CaO* measures the proportion of calcium oxide present in the siliciclastic sediments' silicate fraction. The technique proffered by McLennan et al. (1993) was adopted to determine the CaO* value in this work, where $CaO^*=CaO-(10/3*P_2O_5)$. The index of compositional variability (ICV; Cox et al., 1995) is applied in this study to evaluate the chemical maturity of the Late Cretaceous-Paleocene units and also access sedimentation recycling. The ICV indicator was computed using the equation:

$$ICV = [Fe_2O_3 + K_2O + Na_2O + CaO + MgO + TiO_2]/ Al_2O_3 \quad (5)$$

- place **Figure 3** near here -

- place **Figure 4** near here -

- place **Figure 5** near here -

- place **Figure 6** near here –

3.1. Lithofacies types

Based on representative rock types, color, grain size, bedding pattern, mineral composition and sedimentary structures, 4 lithofacies types have been identified within the two drill cores (Figs. 3 and 5). Lithofacies codes were adapted from Miall (1977, 2006).

3.1.1. Lithofacies I: Mudstone (Fm)

Lithofacies *Fm* is characterized by fine-grained clastic deposits that can be subdivided into laminated and non-laminated mudstones.

3.1.1.1. Laminated mudstone (Fm 1)

The laminated mudstone was identified as the predominant lithofacies in the Mamu and Nkporo formations (samples OW01-09, 11-28, 36 and UB09, 17, 22, 27-33, 36, 39-40 and 42-45). It is typically grey to dark grey, indurated, fissile, poorly to well laminated and carbonaceous. The cumulative thickness of this facies in the Owan-1 and Ubiaja wells are 208 m and 135 m, respectively. Bed thickness varies from 1.0 to >4.0 m. The lithofacies commonly overlies sandstone, shaly sandstone and sandy shale sequences. Little plant material remains and burrows have been found in the shales. The mineral content of this facies is primarily made up of palygorskite, kaolinite, smectite, ankerite, illite, anatase, gypsum, microcline and minor quartz.

3.1.1.2. Non-laminated mudstone (Fm 2)

This subfacies is typically massive, light grey to milky brown, non-fissile and non-carbonaceous. The cumulative thickness of this facies is 55 m in the Owan-1 well (samples OW 10, 30) and 72 m in the Ubiaja well (samples UB 03-06, 18-21). Bed thickness ranges from 2 to >7 m. The

shales are dominated by kaolinite, quartz, calcite, anatase, jarosite, with minor pyrite and hematite.

3.1.2. Lithofacies II: Laminated sandy siltstone and mudrock (Fl)

This lithofacies type varies in color from grey to yellowish-brown with wavy lamination. The particle sizes range from fine sand to silt and clay. The rocks are slightly ferruginized and exhibit bed thicknesses of more than 2 m. The cumulative thicknesses of this facies, usually overlying the mudstone lithofacies, are 63 m and 10 m in the Owan-1 (samples OW 29 and 35) and Ubiaja wells (samples UB 25, 34 and 41), respectively. The mineralogy of this lithofacies is made up of quartz, kaolinite, siderite, and minor amounts of pyrite and hematite.

3.1.3. Lithofacies III: Silt- and mudstone (Fsm)

The *Fsm* lithofacies varies in color from grey to dark brown. The dominant particle sizes are silt and clay sized grains. Individual beds vary from 2 to 7 m in thickness. The cumulative thickness of this facies is 100 m and 44 m in the Owan-1 (samples OW 31-34) and Ubiaja wells (samples UB 08), respectively. The mineralogy of this lithofacies is dominated by quartz, kaolinite, and minor siderite and anatase.

3.1.4. Lithofacies IV: Sandstone (Sh)

This lithofacies type varies in color from milky white to brown and yellow. The grains are angular, sub-rounded to rounded, and poorly to moderately sorted. The major textural

components are silt, and fine to coarse sand grains. Individual bed thicknesses vary from 2 to 16 m. The sandstone facies is dominant in the Ubiaja well (samples UB 01, 02, 07, 10-16, 23-24, 26, 35, 37 and 38), with a cumulative thickness of 161 m. Additionally, the aggregate thickness in the Owan-1 well is up to 40 m. Few plant remains could be identified within the samples. The sandstones are dominated by quartz and minor amounts of hematite and kaolinite.

3.2. Paleoclimate and paleoenvironmental proxies

The ratios Th/U, Rb/Sr, and the C-value are commonly used to reconstruct paleoclimatic variations and have been shown to be reliable (Figs. 3 and 5) (Chang et al., 2013; Li et al., 2021; Zhang et al., 2021). Th/U increases with intense chemical weathering through oxidation and the reduction of U. Generally, values greater than PAAS concentration indicate advanced chemical weathering (McLennan et al., 1993). In contrast, Rb/Sr ratios increase under arid conditions, i.e. low values reflect humid and warm climates, whereas high values suggest arid, dry and hot climatic conditions (Chang et al., 2013; Martinez-Ruiz et al., 2015). Finally, the C-value is based on the fact that the elements Fe, Mn, Cr, Ni, V, and Co are enhanced in humid settings, whereas Ca, Mg, Sr, Ba, K, and Na are concentrated in arid conditions due to precipitation of saline minerals (Hu et al., 2017; Krzeszowska, 2019). A humid paleoclimatic environment is indicated by a high C-value, with C-values > 0.8 indicating humid conditions, 0.6 - 0.8 suggesting semi-humid conditions, 0.4 - 0.6 indicating semi-humid–semiarid conditions, 0.2 - 0.4 indicating semiarid conditions, and C-values <0.2 indicating arid conditions (Figs. 3 and 5; Zhang et al., 2020).

The compositional maturity of sediments and sedimentary rocks is assessed by analyzing their geochemical signatures (Li et al., 2019; Huang et al., 2020; Overare et al., 2020). Commonly, the index of chemical variability (ICV) is utilized for this purpose (Cox et al., 1995). The ternary plot of Fe_2O_3-K_2O-Al_2O_3 indicates Al_2O_3 enrichment, suggesting that clay mineralogy primarily controls the geochemistry of the lithofacies (Fig. 9a; Overare et al., 2020). Clay-rich sedimentary rocks contain high amounts of Al_2O_3 and low concentrations of K_2O, Na_2O and CaO compared to deposits that are poor in clay. Correspondingly, ICV values for clay-rich rocks are higher than for clay-poor rocks. The sedimentary facies with computed ICV values >1 reflect compositional immaturity within the first depositional cycle and active tectonic conditions (Fig. 9c). In contrast, ICV values <1 indicate compositionally matured sediments with high sediment recycling along tectonically inactive plate margins (Long et al., 2012). ICV values in clay minerals (such as montmorillonite and illite) are commonly less than 0.12, 0.13-5 in feldspars and biotite, 5-20 in amphibole and 20-300 in pyroxene due to diminishing Al_2O_3 concentrations (Li et al., 2019).

In the past, a variety of geochemical proxies have been used to assess paleoenvironmental parameters such as paleosalinity, paleoproductivity and the paleoredox conditions in sedimentary rocks (Wei and Algeo, 2020; Wang et al., 2021; Zhang et al., 2021). Sr and Ba ratios, in particular, can provide insights into changes in paleosalinity levels in sedimentary deposits (Moradi et al., 2016; Li et al., 2020) as Sr enrichment is linked to rising paleo-water salinity and salinity rises with depth; thus, high Sr/Ba values indicate rising saltwater depth and salinity (Zhang et al., 2021). As a result, Sr/Ba geochemical signatures have increasingly been recognized as a proxy for paleo-water salinity (Zhang et al., 2021). The Sr/Ba ratio is a reliable proxy for estimating paleosalinity, except in carbonate rocks where Sr could be enriched and

therefore affect the results (Wei and Algeo, 2020). Carbonate fractions typically have much higher Sr concentrations than clay fractions. However, due to the low carbonate mineral content of the studied sections, carbonate-hosted Sr is insignificant for this study (Fig. 9b). As a result, the Sr/Ba ratio can be a valid proxy for paleosalinity interpretation. Commonly, Sr/Ba ratios > 0.5 reflect deposition in a marine environment, 0.2-0.5 indicate brackish water and values < 0.2 point to deposition within a terrestrial environment that is dominated by freshwater (Figs. 3 and 5; Wei and Algeo, 2020; Zhang et al., 2021). The paleosalinity is suggested to substantially affect the growth of organisms, accumulation, and conservation of organic matter (Li et al., 2020).

The trace element ratios of Ba/Al and P/Ti provide valuable information on nutritional conditions and paleoproductivity, i.e. the uptake of dissolved inorganic carbon and its sequestration into organic compounds by primary marine producers (Tribovillard et al., 2006; Algeo et al., 2011; Li et al., 2020; Zhang et al., 2020). Phosphorus is important for all kinds of life on Earth since it is a major component of skeletal material and is involved in a variety of metabolic activities (Li et al., 2020; Zhang et al., 2021). The availability of organic matter is connected to the concentrations of P and Ba in sedimentary deposits, potentially resulting from high productivity (Tribovillard et al., 2006). Because Ti and Al are typically derived from terrigenous detrital matter, Ba/Al and P/Ti ratios are employed to estimate paleoproductivity (Li et al., 2020). Lower productivity is indicated by a P/Ti value of less than 0.34, intermediate productivity is characterized by a P/Ti value of 0.34–0.79, and a P/Ti value of more than 0.79 indicates high productivity (Figs. 3 and 5; Li et al., 2020).

Redox sensitive elements, e.g. V, U, Fe, Mn, Co, Cr, and Ni, indicate the redox characteristics of the depositional environment because they do not move after deposition and

burial. This fact makes these redox-sensitive elements ideal and reliable proxies for interpreting paleoredox conditions of sedimentary rocks (Nath et al., 1997; Guo et al., 2011; Goldberg and Humayun, 2016; Li et al., 2018a; Xi and Tang, 2021). In this study, the trace element ratios V/Cr, Ni/Co, U/Th, and V/(V+Ni) that are widely applied were utilized to assess the paleoredox setting. Hu et al. (2017) used Ni/Co, U/Th, V/Cr, and V/(V+Ni) as paleoredox indicators to investigate the sedimentary paleoredox conditions in the Zhanjin Formation of China's Qiangtang Basin. Furthermore, Li et al. (2021) used Ni/Co, V/Cr, and V/(V+Ni) as geochemical proxies to reconstruct the paleoredox conditions in the Hanjiawu Formation of China's Santanghu Basin. In addition, the proxies stated above have been successfully applied in the reconstruction of paleoenvironmental settings in other WCARS basins (Tan et al., 2017; Lai et al., 2018; Adeoye et al., 2020; Overare et al., 2020; Abubakar et al., 2021). Anoxic, dysoxic, and oxic environments were defined using reference standards for U/Th, V/Cr, Ni/Co, and V/(V + Ni) (Figs 4 and 6). Commonly, V/Cr ratios >4.25 signify an anoxic depositional environment, i.e., exhibit strong reducing conditions. Ratios between 2.0 - 4.25 indicate a dysoxic depositional setting, i.e. reducing conditions. Finally, ratios <2.0 point to an oxic depositional environment, i.e. oxidizing conditions (Li et al., 2018b). Similarly, Ni/Co values >7.0 show an anoxic depositional environment, 5.0 - 7.0 indicates a dysoxic environment, and <5.0 suggests oxic conditions (Figs 4 and 6; Jones and Manning, 1994; Guo et al., 2011). U/Th ratios >1.25 indicate anoxic conditions, 0.75 – 1.25 reflect dysoxic conditions, and <0.75 show oxic conditions (Jones and Manning, 1994). Finally, V/(V+Ni) ratios >0.84 indicate euxinic depositional conditions, i.e. anaerobic-reducing conditions, 0.54 – 0.82 indicates anoxic settings, and 0.46 – 0.60 indicates dysoxic depositional conditions (Figs. 4 and 6; Hatch and Leventhal, 1992).

Zr is a common continental inert element that is preserved in continental, transitional and shallow-marine environments (Pehlivanli, 2019). Rb is a common mobile element during a variety of different geological processes, and it is accumulated in deep water with low energy because of its active chemical properties (Li et al., 2018b). As a result, the Zr/Rb ratio can react to changes in water depth and therefore it is considered a good indicator for paleo-hydrodynamics (Figs. 4 and 6; Teng, 2004; Teng et al., 2005; Zhao et al., 2016; Li et al., 2018b; Pehlivanli, 2019). The lower the Zr/Rb ratio, the greater the water depth and the weaker the hydrodynamic pressure (Li et al., 2018b; Pehlivanli, 2019). A higher Zr/Rb ratio indicates shallow water circulation and stronger hydrodynamic pressure. Teng (2004), Zhao et al. (2016), and Li et al. (2018b) applied the Zr/Rb indicator to determine the hydrodynamic characteristics of the Zhuozishan, Shanxi and Yanchang Formations in the Ordos Basin of China, and their data revealed weak and comparatively strong paleo-hydrodynamic influences during the deposition of the mudrocks. The Zr/Rb ratio <0.92 shows a weak paleo-hydrodynamic regime, 1.25 - 4.76 means intermediate to strong hydrodynamic pressure, and > 4.76 indicates a strong paleo-hydrodynamic regime (Teng, 2004; Pehlivanli, 2019).

Fe and Mn major elements possess entirely different characteristics regarding the transportation and sedimentation process in the sedimentary basin due to their chemical properties (Wang et al., 2020). Although the Fe element is easily oxidized and precipitated, the Mn is a major stabile element that can be transferred to deep water regions far away from the seashore (Wang et al., 2020). Because the Fe/Mn ratio has a strong relationship with water depth, it can be used to classify paleowater depth, with higher ratios indicating shallower water conditions (Figs. 4 and 6; Toyoda, 1993; Takamatsu et al., 2000; Wang et al., 2020).

4. Results

4.1. Sedimentary bulk-rock geochemistry

The major element oxides SiO_2 and Al_2O_3 constitute the dominant oxides, with contents ranging from 7.08 - 72.87 wt.% and 2.65 - 22.63 wt.% in the Owan-1 well and from 46.15 - 85.22 wt.% and 4.13 - 27.42 wt.% in the Ubiaja well (electronic supplementary material 1). The concentrations of Fe_2O_3, MgO and CaO in the Owan-1 well vary between 1.19 - 23.85 wt.%, 0.18 - 8.09 wt.% and 0.13 - 47.37 wt.%, respectively. In the Ubiaja well, they range from 0.70 - 10.77 wt.%, 0.08 - 0.54 wt.% and 0.04 - 0.49 wt.%, respectively. Na_2O, K_2O, P_2O_5, TiO_2 and MnO are available in small concentrations of less than 2%. The CIA values for the Owan-1 and Ubiaja samples (ranging from 78 to 99) are higher than the PAAS (70) and UCC (52). Similarly, the PIA values for the studied sections (ranging from 81 to 100) record higher values relative to the PAAS (79) and UCC (53). With the exception of sample OW 10, which exhibits a CIW of 81, the CIW for these samples ranges from 81 to 100, which is higher than PAAS (82) and higher than UCC (58). The C-values of the analyzed samples vary between 0.6-4.2 and 0.1-3.9 for the Ubiaja and Owan-1 rocks respectively.

According to the classification scheme by Sprague et al. (2009), the samples from the Owan-1 well can be chemically classified as claystones (OW 1, 10, 11, 14, 21, 26, 29, 30) and siltstones (OW 36, 31) (Fig. 7a). In contrast, the Ubiaja well samples are classified as claystones (UB 3, 17, 30, 32, 40), argillaceous sandstones (UB 21) and sandstones (UB 7, 9, 25, 34). Therefore, the geochemical classification agrees with the petrographical classification (see section 3.1). Correspondingly, the classification system by Herron (1988) shows that all samples can be classified as Fe-shales, Fe-rich sands and shales, with most of the samples plotting in the Fe-

shale field (Fig. 7b), which can probably be attributed to their pyrite, hematite and siderite contents.

The SiO_2 content within the samples suggest detrital and biogenic contributions (Fig. 7c). The exact detrital influence was determined by the geochemical proxy D* = Al/(Al+Fe+Mn) (Boström, 1970; Barbera et al., 2006), which links Al_2O_3, found in the continental crust (i.e. D*=0.79; Taylor and McLennan, 1985; Barbera et al., 2006), with MnO and Fe_2O_3, as typified by the oceanic crust affinity (i.e. D*=0.68; Taylor and McLennan, 1985; Barbera et al., 2006). The detrital characteristics and continental crust source for the deposits in this study range from 0.43 to 0.95 D* (mean, 0.82 D*) for the Ubiaja well and from 0.32 to 0.88 D* (mean, 0.74 D*) for the Owan-1 well (supplementary electronic material 1), indicating a strong continental influence during the deposition of the sediments at the western margin of the Anambra Basin. The silica in our study is mainly sourced from terrigenous detrital quartz with minor biogenic input. The biogenic silica input is possibly from diatoms and other siliceous plankton, which are common sources of biochemically precipitated silica in marine environments, indicating an abridged period of comparatively shallow to deep depositional conditions remote from terrigenous input for mudrocks along the shore (Kidder and Erwin, 2001; Adeoye et al., 2020).

The major sources of trace elements in sedimentary basins are terrestrially weathered rocks, plankton remnants, and hydrothermal fluids (Tribovillard et al., 2006; Adeoye et al., 2020). The trace element geochemistry of sedimentary deposits has been proven to contain significant information on paleoenvironmental settings, and this has been utilized worldwide in interpreting depositional settings of ancient sedimentary rocks (Tribovillard et al., 2006; Wei and Algeo, 2020; Wang et al., 2021; Xi and Tang, 2021; Zhang et al., 2021). In this contribution, the trace elemental concentrations were used to determine the paleoclimate, paleosedimentary

environment, paleogeographic redox conditions, hydrodynamic pressure and paleowater depth of the studied formations. The stratigraphic variations of trace element ratios and paleogeographic redox indicators in the Imo, Mamu and Nkporo formations are shown in Figs. 3 to 6. Furthermore, we focused on the mudrocks since elemental geochemistry proxies and threshold limits have primarily been established and applied in marine-transitional shales and mudrocks and provide reliable interpretation (Zhang et al., 2021).

The enrichment factor (EF) is commonly used to assess the degree of element enrichment (Li et al., 2018b). It is calculated as the proportion of an element's concentration in the samples to the equivalent value of UCC (Rudnick and Gao, 2003). REE and trace element patterns (Fig. 8) show enriched and depleted concentrations normalized to chondrite (Taylor and McLennan, 1985) and UCC (Rudnick and Gao, 2003).

- place **Figure 7** near here -

- place **Figure 8** near here -

- place **Figure 9** near here -

5. Discussion

5.1. Paleoclimate and paleoenvironment

The geochemistry and mineralogy of clastic sedimentary deposits are strongly influenced by the existence and degree of chemical weathering (Liu et al., 2009; Krzeszowska, 2019; Bokanda et al., 2021), and a variety of different weathering indicators can be used to assess the degree of sedimentary rock weathering (Parker, 1970; Nesbitt and Young, 1982, 1984; Harnois, 1988;

Fedo et al., 1995). Apart from a simple statement on the weathering conditions, these weathering indicators can also be used as parameters to understand the climatic conditions during deposition. Low degrees of weathering usually correspond to arid or cool and dry climatic conditions, whereas high degrees of weathering are generally interpreted as being related to humid temperate to tropical conditions (Visser and Young, 1990; Chen et al., 2021b). All three weathering indicators that have been used for this study (CIA, PIA, CIW) are relatively high (higher than UCC and PASS) and are therefore an indication of high degrees of weathering as can be found in humid tropical environments (Chen et al., 2021b). The high degree of weathering is also supported by the abundance of clay minerals such as kaolinite, smectite, and palygorskite (Liu et al., 2009). An exception is formed by sample OW10 with a CIA value of 78, indicating a moderate degree of chemical weathering.

To support the evidence from these conventional parameters, a variety of other geochemical indicators of climate changes are applied to understand the Late Cretaceous-Paleogene paleoclimate of the Anambra Basin. Previous research has shown that paleoclimatic conditions at the time of deposition can be deduced from the relative concentration and distribution of trace elements in mudrocks (Hu et al., 2017; Zhang et al., 2020; Wei et al., 2021).

The Th/U, Rb/Sr and C-values used in this study corroborate with the CIA, PIA and CIW data, thus supporting deposition in a humid tropical environment (Chang et al., 2013; Chen et al., 2021b; Zhang et al., 2021). The Th/U ratios of most of the analyzed samples are higher than the average upper crustal value (avg. 4.0 and 3.7 for the Ubiaja and Owan-1 rocks, respectively). Similarly, the Rb/Sr proxy and C-Values reveal a warm and humid environment (Figs. 3 and 5). The C-values are dominantly high, suggesting a warm and humid palaeoclimate. A few *Fm* lithofacies in this study reveal low C-values, i.e. 0.1-0.8 (OW 10 and 11) and 0.6-0.8 (UB 32 and

40), reflecting semi-humid-arid palaeoclimatic conditions. Ejeh (2021), based on subsurface data from the Amansiodo-1 well, interpreted a warm, humid and hot arid paleoclimate in the basin's eastern segment.

The Cretaceous period is known to have experienced extreme temperature conditions (Hay and Floegel, 2012). From the Early to Late Cretaceous, global temperature records show sustained high temperatures, preceded by cooling towards the end of the Cretaceous period (Ladant et al., 2020). Reconstruction of paleo-CO_2 levels in the Cretaceous reveals that CO_2 and temperatures peaked during the Cenomanian-Turonian before declining throughout the upper Cretaceous, paleogeographic shifts and greater CO_2 amounts in the atmosphere were postulated as the main causes of warm Cretaceous temperatures (Ladant et al., 2020). There was abundance of rainfall throughout West Africa in the Cretaceous, which suggests the possibility of intense chemical weathering (Sellwood and Valdes, 2006). Data from Bolarinwa et al. (2019) recorded δ^2H (-50.80 and - 66.40%) and $\delta^{18}O$ (15.40 and 21.20%) values that reveal high-temperature conditions typical of warm tropical climates (25–40°C) for the Cretaceous formations in the Benue Trough of Nigeria. Our present study corroborates the δ^2H and $\delta^{18}O$ values from the Maastrichtian deposits in the Lower Benue Trough with similar depositional conditions of the Anambra Basin, which formed under significantly warmer climatic conditions than the present (Bolarinwa et al., 2019; Edegbai et al., 2019a). Additionally, Chumakov et al. (1995) interpreted the Maastrichtian paleoclimate of West Africa to be predominantly warm and tropical, which supports our interpretations. According to recent calculations, tropical temperatures during the Cretaceous period ranged from 22-34°C (Scotese et al., 2021), with the highest temperatures recorded in the Cenomanian-Turonian period (~34°C).

The paleoenvironmental interpretation of the identified lithofacies as described in section 3.1 is given in Figures 3 and 5. The fine particle size of the *Fm 1* lithofacies and the parallel lamination reflects deposition in a relatively quiet depositional setting with a low sedimentation rate. Carbonaceous and non-carbonaceous mudrocks dominate this facies in our study. The shales were transported and deposited in a low to high energy hydrodynamic setting, most probably in a deltaic and marginal marine depositional setting with incessant energy variations. According to Miall (2006), the described sediments reflect deposition in delta plain settings, comprising non-marine to brackish environments and estuary and tidal flats to interdistributary bays (Miall, 2006). Therefore, this subfacies are interpreted as marginal marine facies (Miall, 1977; Beukes, 1987; Dim et al., 2019).

Like the subfacies described before, the non-laminated mudstone facies (*Fm 2*) were deposited under low to medium transport energy conditions, either in a coastal swamp or a relatively distal marginal marine environment (Miall, 1978).

The *Fl* facies, characterized by laminated silt, shale and very fine-grained sand with wavy lamination, indicates a variation in the depositional energy. Similar facies were interpreted as deposits accumulated in a tidal channel marsh to an intertidal environment with variation in depositional energy, resulting in the typical grain size variation (Walker and Cant, 1984; Onuigbo et al., 2012).

The particle distribution of the *Fsm* lithofacies suggests deposition under low to medium energy hydrodynamic conditions. Similar facies were interpreted to have accumulated either in a delta front setting or an open shelf environment (Miall, 1977, 2006; Dim et al., 2019).

The particle size of the *Sh* lithofacies is suggestive of medium to relatively high transport energy conditions. This lithofacies unit is therefore interpreted as being deposited within a tidal flat to shelf environment (Miall, 1997; Onuigbo et al., 2012).

5.2. Geochemical maturity

The analyzed samples from the Ubiaja and Owan-1 wells generally exhibit ICV values <1, suggesting a high influence of sediment weathering and transport over a long distance under humid conditions (Figs. 9b and 9c). Only a few exceptions in the Owan-1 well (OW 10 and 29) show higher values than 1 and therefore imply the existence of immature sediments. All the lithofacies in our data show a similar maturity trend. The ICV values reflect intense weathering of source rocks and paleosedimentary climate variations during deposition. The ICV values generally increase with increasing weathering intensity in a humid climate and can therefore be correlated to the weathering indices discussed in section 5.1 (Figs. 3 and 5).

The dominance of matured deposits at the western margin of the Anambra Basin suggests intense weathering conditions, and the provenance of the mudrocks indicates a passive plate tectonic setting (Long et al., 2012; Hong et al., 2020). Overare et al. (2020) recently assessed the geochemical maturity of the Mamu Formation at the eastern margin of the Anambra Basin. Their data revealed similar results, thus pointing towards clay-rich, matured sediments in an inactive tectonic plate margin. The trace elemental composition of the Th/Sc *vs.* Zr/Sc plot supports this hypothesis, indicating a geochemical trend showing compositionally matured mudrocks (Fig. 9d).

5.3. Paleoproductivity and paleoredox conditions

Paleoproductivity indicates the quantity of organic matter that organisms can generate per unit area and time during the energy cycle (Chen et al., 2021a). Previous studies have shown that low Ba/Al and P/Ti ratios generally indicate low paleoproductivity and significant siliciclastic dilution in an oxic environment (Zhang et al., 2020; Li et al., 2020).

Within the studied succession intersected by the Owan-1 and Ubiaja wells, the Ba/Al and P/Ti ratios for the Imo, Mamu and Nkporo formations are lower than typically laminated mudrocks (Zeng et al., 2015; Li et al., 2020). The P/Ti values for all the lithofacies are below 0.34, indicating low primary productivity (Figs. 3 and 5). The Ba/Al ratio in the Ubiaja and Owan-1 rocks shows low values from the base to the top, indicating low paleoproductivity, except for sample UB 34 (Ba/Al value of 86.3), signifying moderate paleoproductivity. A humid climate can increase primary productivity because nutrient limitations in the marine environment are often drawn from the terrestrial environment (Xin et al., 2021). However, despite providing adequate biological nutrition, influx can also dilute organic matter (Chen et al., 2021a). Nevertheless, our data show a low primary paleoproductivity for the studied sections, which is possibly due to a high detrital flux together with a turbulent water body, and shallow water depth with a high energy, an oxidizing environment that is unfavorable to high paleoproductivity (Yan et al., 2018; Zhang et al., 2019; Wei et al., 2021). In addition, although humid climates with high weathering conditions can increase the nutrient supply in the marine environment, oxic conditions together with high amounts of terrigenous material can dilute the organic matter content in sediments, thus affecting the paleoproductivity during deposition of the mudrocks (Cheng et al., 2021; Chen et al., 2021a; Wei et al., 2021).

Trace elements in sedimentary environments react to redox fluctuations in relatively predictable patterns. Evaluating ambient paleoredox conditions requires a suite of trace elements

rather than a single element index. The investigation of paleoredox conditions by the applied indicators of the two studied wells revealed comparable results: the lower Campanian Nkporo Formation, the Maastrichtian Mamu Formation, and the Paleocene Imo Formation reveal oxic environmental conditions (Figs. 4 and 6). The V/Cr values in the Campanian, Maastrichtian and Paleocene lithofacies in the Ubiaja well increase gradually from the base to the top, with all the lithofacies showing low values, i.e. <2.0. The Maastrichtian Mamu and the Paleocene Imo units in the Owan-1 well record higher V/Cr values relative to the Ubiaja well. Similarly, the U/Th ratios for the Campanian Nkporo, the Maastrichtian Mamu, and the Paleocene Imo formations in the Ubiaja well record low values, i.e., average 0.25, 0.27 and 0.25, respectively. Furthermore, the Ni/Co ratios in this study record low values, i.e. <1.9. Ejeh's (2021) data revealed similar values from the Amansiodo-1 well. The V/Cr, U/Th and Ni/Co ratios consistently reveal strong oxic depositional conditions during the Late Cretaceous-Paleocene sedimentation period in the studied well sections except sample OW 30 (U/Th value of 0.79), signifying a dysoxic setting. However, the V/(V + Ni) ratios show prevailing lower oxygen concentrations (Hatch and Leventhal, 1992). The majority of lithofacies show V/(V + Ni) ratios above the threshold limit, i.e. V/(V+Ni) >0.6, except sample UB 09 (V/(V + Ni) ratio of 0.49), thus indicating dysoxic/anoxic conditions, which suggests that the water column was not entirely under oxic conditions throughout the formation of the Imo, Mamu and Nkporo formations. The discrepancy between the V/(V+Ni) and other indicators can also be attributed to processes other than redox conditions, such as sediment recycling, sedimentation rates, depositional and subsequent diagenetic processes, all of which can affect the metal concentration (Wang et al., 2017; Han et al., 2020). Therefore, paleoredox indicators should be applied with care when determining the redox conditions.

Low authigenic U enrichment suggests that the studied mudrocks were mostly deposited in oxic or suboxic environments (Tribovillard et al., 2006). The sedimentary facies of the Owan-1 and Ubiaja samples show enrichment in U and V, indicating euxinic depositional conditions in the water column (Fig. 8a) (Tribovillard et al., 2006). V and Cr concentrations are often depleted to UCC values, implying overall oxic bottom water conditions (Fig. 8a) (Kloss et al., 2015). Overare et al. (2020) postulated similar conditions at the eastern margin of the Anambra Basin. In a recent study, Ejeh (2021) reported an oxic paleo-redox environment for the Late Cretaceous formations from the Amansiodo-1 well in the central-eastern segment of the Anambra Basin. The paleosedimentary redox proxies applied in this study show a similar trend and pattern in both wells. The paleoredox conditions determined from V/Cr, U/Th, and Ni/Co ratios show a good agreement. The paleoenvironmental conditions in the Imo, Mamu and Nkporo formations are reconstructed as primarily oxic with minor dysoxic conditions, based on paleoredox index values.

In addition, the Cu/Zn ratio is used to define the depositional environment further. High Cu/Zn ratios in a sedimentary environment reflect reducing depositional conditions, whereas low Cu/Zn values indicate oxidizing depositional conditions (Hallberg, 1976). Consequently, the low Cu/Zn ratios recorded for the Ubiaja (averaging 0.38) and Owan-1 mudrocks (averaging 0.11) indicate that the different lithofacies of the three studied formations were all accumulated in an oxidizing depositional environment. Our data compare favorably with previous works in the Anambra Basin and thus support the interpretation of dominantly oxic conditions (Gebhardt, 1998; Adebayo et al., 2015; Edegbai et al., 2020; Overare et al., 2020; Ejeh, 2021).

5.4. Paleohydrodynamics and paleowater depth/paleosalinity

Paleohydrodynamics describe the energy conditions of the water mass during the deposition of ancient sedimentary rocks in the aquatic environment (Pehlivanli, 2019). In this study, we utilized the Zr/Rb ratio to detect the paleohydrodynamic conditions during the deposition of Late Cretaceous-Paleocene formations in the Anambra Basin (Figs. 4 and 6). The Zr/Rb ratio in the lower depth interval of the Ubiaja well, representing the Nkporo Formation, recorded lower values than the Mamu Formation. The Maastrichtian Mamu Formation in the Owan-1 well shows lower paleohydrodynamic values compared to the Ubiaja well, indicating a strong hydrodynamic regime for the basal units and a gradual transition to intermediate hydroenergy at the top, as shown from the Zr/Rb values (cf., Li et al., 2018b). Our data therefore reveal a predominantly strong hydrodynamic regime and shallow sedimentary water circulation during the deposition of the Mamu and Imo formations. A cross plot of Sr/Ba ratios *vs.* the hydrodynamic proxy (Zr/Rb) (supplementary electronic material 2) shows a very weak correlation between paleosalinity and hydrodynamics, suggesting that there is no direct relationship between paleosalinity and paleohydrodynamics in the studied sections.

Overall, the Fe/Mn ratios show relatively high values in the Campanian Nkporo Formation in the Ubiaja well. The Maastrichtian Mamu Formation shows slightly higher values than the Nkporo and Imo formations. The Mamu Formation in the Owan-1 well shows similar values. The Imo Formation reveals similar values except OW 10, which records a Fe/Mn ratio of 6, thus indicating a deep paleowater. Throughout the succession, the seawater became gradually shallower (Fig. 6), which is consistent with other data (Ubiaja well) from the Maastrichtian. The high Fe/Mn ratios recorded in this study suggest a prevailing shallow paleowater depth during the deposition of the Imo, Mamu and Nkporo formations. Similar deductions of the paleowater depth in the Maastrichtian were drawn by Edegbai et al. (2020). The authors inferred shallow

water depths for the Trans-Saharan Seaway in the Cretaceous during the deposition of the Mamu Formation in the Anambra Basin from palynofacies data, which is consistent with our present study. The paleowater depth corroborates the hydrodynamic influence detected in this study, indicating intense hydrodynamic pressure in a shallow water circulation.

Paleosalinity is an important indicator that is used to reflect the sedimentary environment of the water column in the geologic history (Cheng et al., 2021). In the Owan-1 and Ubiaja mudrocks, the Sr/Ba ratios fluctuate from the Campano-Maastrichtian to the Paleocene (Figs. 3 and 5). The results show that the Campanian Nkporo Formation (average Sr/Ba values of 0.19) was formed in a brackish to freshwater environment. The *Fm* lithofacies in the Ubiaja well record the highest paleosalinity values. Upwards through the stratigraphy, the values gradually increase, thus depicting the transition from freshwater to brackish, then to marine, and finally back to brackish conditions, which can be seen as a shift towards deltaic deposition. The Mamu and Imo formations in the Ubiaja well show relatively constant paleosalinity values throughout the Maastrichtian-Paleocene with average values of 0.32 and 0.5, indicating ongoing sedimentation in a brackish water environment.

In the Owan-1 well, the Mamu and Imo formations generally exhibit higher Sr/Ba values than the Nkporo, Mamu and Imo formations in the Ubiaja well (average of 4.71). The paleosalinity at the base of the Owan-1 well is low and gradually increases towards the top, as shown by the Sr/Ba values (Fig. 5), suggesting a lower sea level and more negligible seawater effect during sedimentation of the basal units. The Imo Formation formed in a marginal shallow-marine environment. The Mamu Formation was deposited in a proximal shallow-marine environment. Our data indicate comparatively high levels of salinity in the studied well sections. The Campanian Nkporo Formation formed in a brackish to freshwater environment, the Mamu

Formation was deposited in a brackish to shallow-marine environment, and the Imo Formation formed in a marginal marine environment (Figs. 3 and 5), thus supporting the hypothesis that the Anambra Basin was formed in a deltaic setting (Nwajide and Reijers, 1996; Odunze et al., 2013; Uzoegbu et al., 2013; Abubakar, 2014).

Water salinity is usually influenced by the environment. Hot and arid climates commonly have high evaporation rates, resulting in high salinity, whereas warm and humid climates have lower evaporation rates, resulting in lower salinity (Wei et al., 2021). We performed a cross plot of Sr/Ba *vs.* C-value (supplementary electronic material 2) and found no consistent salinity trend in the dataset of the Owan-1 and Ubiaja wells, indicating that the paleoclimate did not play a significant role in the marginal basin's salinity fluctuation. In addition, we observed a very weak correlation between paleosalinity and paleowater depth, suggesting that there is no direct relationship between salinity and water depth in the studied sections.

5.5. Paleoenvironmental implications

A critical part of the study is to understand the paleoenvironment of the Anambra Basin and the relationship with the development of the Benue Trough, the Western and Central African Rifts (WCARS) and the South Atlantic during the Cretaceous. The WCARS are related to extensive fracture structures that extend from Nigeria's Benue Trough, the Niger Graben Basin, and the grabens of Chad and Sudan. The Anambra Basin and Benue Trough are related structures that are part of the WCARS (Abubakar, 2014). The formation of the WCARS is strongly connected to the opening of the South Atlantic Ocean in the Early Cretaceous (130-119 Ma), with rifting spreading far into Africa through the Benue Trough (Fairhead, 1988). The Niger, Chad, Sudan, and Nigeria WCARS basins are extensive and consist of Cretaceous marine siliciclastic sediments with minor volcanic rocks. The sedimentation period of the Cretaceous Mamu and

Nkporo formations in the Anambra Basin was less affected by biochemical deposition, as reflected by the high Fe_2O_3+Al_2O_3 values relative to the CaO+MgO contents, which supports the influx of terrigenous clastics in the Anambra Basin (Wei et al., 2021). During the Maastrichtian, the Trans-Saharan Seaway was re-established for the second time, and the connection line propagated westward over the Bida Basin, which connects the Anambra Basin and extends to the Atlantic Ocean (Edegbai et al., 2019b). The geochemistry of the Bida Basin and Benue Trough is similar to those reported in this study and less affected by biochemical deposition, supporting our data. This study infers paleoclimate conditions from lithofacies revealing dominantly humid tropical environments except for a few *Fm* lithofacies that correspond to semi-humid-arid environments. For the Mamu and Nkporo formations, it can be observed that the persistent humid tropical conditions matched the Campanian-Maastrichtian general climatic trend (Chumakov et al., 1995; Sellwood and Valdes, 2006; Hay and Floegel, 2012). The paleoclimate reconstructions of this study are similar to other WCARS basins. Palynological investigations of the Bida Basin revealed palm pollen as well as spores of *Acrostichum aureum* and pteridophytes, indicating a humid tropical climate, with predicted paleo-vegetation ranging from savanna to rainforest (Ojo and Akande, 2008; Onoduku et al., 2017). The Sekuliye shales in the Benue Trough also indicate deposition in a humid setting, in a brackish to shallow-marine environment with oxic conditions (Abubakar et al., 2021). The Aradeiba Formation in the Muglad Rift Basin (Sudan) formed under warm, humid tropical environments where high precipitation occurred during the Early Cretaceous (Leyuan et al., 2021). The warm-humid tropical climate was also dominant in the Termit Basin (Niger-Chad region) in the Late Cretaceous during the sedimentation of the Yogou Formation, as inferred from high ω(MgO)/ω(CaO) fractions, high CIA, and low Sr/Cu values (Lai et al., 2018). In addition, the Bongor Basin in Chad shows both

warm, humid and hot arid paleoclimates as inferred from trace element geochemistry. The palynoflora similarly points to arid climatic conditions (Tan et al., 2017). Intense weathering and geochemically matured sediments are prevalent in the Anambra Basin, as inferred from elemental chemistry proxies (Ejeh, 2021). This is consistent with data presented by Sellwood and Valdes (2006) that reveal high amounts of rainfall during the Cretaceous period in West Africa. Abundant rainfall in a tropical environment favors chemical weathering of rocks and sediment recycling and thus reflects geochemical matured sediments (Cox et al., 1995). The lithofacies show deposition in a shallow-water environment with strong hydrodynamic conditions. The depth of the Trans-Saharan Seaway in the Cretaceous was determined to be shallow by Edegbai et al. (2020). The Trans-Saharan Seaway was a key supplier of sediments for the Anambra Basin. According to Ojo et al. (2021), the Maastrichtian Sea of the Bida Basin was shallow, short-term and disrupted by periodic river runoffs. This is consistent with our findings, which suggest that shallow water depths with considerable hydrodynamic effect existed in the Anambra Basin throughout the Campanian-Maastrichtian. The lithofacies show moderate to high paleosalinity, indicating that deposition took place in a brackish to shallow-marine environment. The primary reason for this environment is that the Mamu and Nkporo formations were deposited due to the re-establishment of the Trans-Saharan Seaway and its link with the Tethys and the Atlantic Ocean during the Campanian-Maastrichtian (Edegbai et al., 2020). The geochemical proxies used to interpret the paleoproductivity all point to low primary productivity ($P/Ti < 0.34$), which can be linked to a strong hydrodynamic regime, shallow water depth, and input of terrestrial detritus, which negatively affected blooms of planktonic organisms (diatoms etc.), resulting in a decrease in primary productivity.

The mostly oxic conditions detected in this study reflect shallow-water environments in the Anambra Basin, where high oxygen levels persisted during deposition. Furthermore, the basin experienced slow sedimentation and intense sediment recycling during the deposition of the Mamu and Nkporo formations. The variation in paleosalinity and depositional redox conditions might be linked to paleogeographic locations where detrital influx varies, resulting in variable redox hydrodynamic and water conditions (Edegbai and Schwark, 2020).

The Anambra Basin and the other WCARS basins share similarities in paleoweathering, paleoclimate, paleowater depth, paleosalinity, and paleoredox conditions despite differences in sediment provenance, paleogeographic locations, and the exposure of some WCARS basins to thermal fracture and crustal upheaval. Depositional settings varied during the formation and sedimentation of these basins and are significantly more important than later alterations, since there are only minor changes in the inorganic geochemical fingerprints of these WCARS basins.

6. Conclusions

Major oxides, trace elements, REE, mineralogy, and lithofacies data have been used to investigate paleoclimate, paleosalinity, as well as paleohydrodynamic and paleoenvironmental conditions of the hydrocarbon prospective Campano-Maastrichtian and Paleocene formations of the southwestern Anambra Basin. The dominance of kaolinite and quartz minerals, together with weathering and paleoclimate proxies, such as CIA, PIA, CIW, ICV, Th/U, Rb/Sr, and C-value, indicate that the Late Cretaceous-Paleogene Nkporo, Mamu and Imo formations were subjected to intense weathering throughout the Maastrichtian-Paleocene in a warm, humid and tropical climate with only short-term semi-humid and semi-arid conditions in the Late Cretaceous.

Compared to other WCARS basins, geochemical data from the Anambra Basin indicate that the basins dominantly formed under humid tropical climatic conditions.

The Sr/Ba, Ba/Al, and P/Ti ratios indicate that the Nkporo and Mamu mudrocks of the Anambra Basin were deposited under brackish to saline environments and with low primary productivity due to the influx of terrestrial clastic materials and strong hydrodynamic conditions.

Despite the presence of dark grey carbonaceous *Fm* lithofacies, geochemical proxies indicate that anoxic conditions only occurred sporadically. This could have had an effect on organic matter accumulation in the studied succession, lowering the hydrocarbon potential at the basin's southwestern margin. Wavy laminations are found in *FI* lithofacies, indicating retreating seawater and significantly high hydrodynamic environments. Ultimately, the Imo, Mamu and Nkporo formations of the southwestern Anambra Basin represent deposits of a shallow Campano-Maastrichtian seaway, comparable with the Maastrichtian Patti Formation of the adjacent Bida Basin in the north.

Declaration of interest

None

Acknowledgements

E.J.O. and N.L. thank the University of Pretoria for financial support. R.Y acknowledges the China-ASEAN Maritime Cooperation Fund Project (grant No.12120100500017001) and the National Natural Science Foundation of China (grant No. 41972146) for financial support. We thank Reuben Okoliko of the Nigerian Geological Survey Agency for providing access to the ditch/core samples. The reviews of two anonymous reviewers significantly improved the

manuscript and are gratefully acknowledged. Editor Shucheng Xie is thanked for handling our manuscript.

References

Abubakar, M.B., 2014. Petroleum potentials of the Nigerian Benue Trough and Anambra Basin: a regional synthesis. Natural Resources 2014.

Abubakar, U., Usman, M.B., Aliyuda, K., Dalha, A., Bello, A.M., Linus, L.N., 2021. Major and trace element geochemistry of the shales of Sekuliye Formation, Yola Sub-Basin, Northern Benue Trough, Nigeria: implications for provenance, weathering intensity, and tectonic setting. Journal of Sedimentary Environments 6, 473–484. https://doi.org/10.1007/s43217-021-00067-2

Adebayo, O.F., Adegoke, A.K., Mustapha, K.A., Adeleye, M.A., Agbaji, A.O., Abidin, N.S.Z., 2018. Paleoenvironmental reconstruction and hydrocarbon potentials of Upper Cretaceous sediments in the Anambra Basin, southeastern Nigeria. International Journal of Coal Geology 192, 56–72.

Adebayo, O.F., Akinyemi, S.A., Ojo, A.O., 2015. Palaeoenvironmental studies of Odagbo coal mine sequence, Northern Anambra Basin, Nigeria: insight from palynomorph and geochemical analyses. International Journal of Current Research 7, 20274–20286.

Adeleye, M.A., Daramola, D.A., 2018. Organic Source Input, Thermal Maturity and Paleodepositional Conditions of Imo Formation in the Anambra Basin, Nigeria. Conference of the Arabian Journal of Geosciences. Springer, 161–164.

Adeoye, J.A., Akande, S.O., Adekeye, O.A., Abikoye, V.T., 2020. Geochemistry and paleoecology of shales from the Cenomanian-Turonian Afowo formation Dahomey

Basin, Nigeria: Implication for provenance and paleoenvironments. Journal of African Earth Sciences 169, 103887. https://doi.org/10.1016/j.jafrearsci.2020.103887

Agagu, O.K., Adighije, C.I., 1983. Tectonic and sedimentation framework of the lower Benue Trough, southeastern Nigeria. Journal of African Earth Sciences 1, 267–274.

Akaegbobi, I.M., Nwachukwu, J.I., Schmitt, M., 2000. Chapter 17: Aromatic Hydrocarbon Distribution and Calculation of Oil and Gas Volumes in Post-Santonian Shale and Coal, Anambra Basin, Nigeria, in: Mello, M.R., Katz, B.J. (Eds.), Petroleum Systems of South Atlantic Margins: American Association of Petroleum Geologists Memoir 73, pp. 233-245.

Akande, S.O., Mücke, A., 1993. Depositional environment and diagenesis of carbonates at the Mamu/Nkporo formation, anambra basin, Southern Nigeria. Journal of African Earth Sciences (and the Middle East) 17, 445–456.

Akinyemi, S.A., Adebayo, O.F., Ojo, O.A., Fadipe, O.A., Gitari, W.M., 2013. Mineralogy and geochemical appraisal of paleo-redox indicators in Maastrichtian outcrop shales of Mamu formation, Anambra Basin, Nigeria. Journal of Natural Sciences Research 3, 48–64.

Algeo, T.J., Kuwahara, K., Sano, H., Bates, S., Lyons, T., Elswick, E., Hinnov, L., Ellwood, B., Moser, J., Maynard, J.B., 2011. Spatial variation in sediment fluxes, redox conditions, and productivity in the Permian–Triassic Panthalassic Ocean. Palaeogeography, Palaeoclimatology, Palaeoecology 308, 65–83.

Anakwuba, K.E., Onyekwelu, C.U., 2010. Subsurface sequence stratigrphy and reservoir characterization of the Southern part of Anambra Basin, Nigeria. AAPG Search and Discovery.

Antolinez-Delgado, H., Oboh-Ikuenobe, F.E., 2007. New species of dinoflagellate cysts from the Paleocene of the Anambra basin, southeast Nigeria. Palynology 31, 53–62.

Barbera, G., Mazzoleni, P., Critelli, S., Pappalardo, A., Lo Giudice, A., Cirrincione, R., 2006. Provenance of shales and sedimentary history of the Monte Soro Unit, Sicily. Periodico Di Mineralogia 75, 313–330.

Bello, R., Ofoha, C.C., Wehiuzo, N., 2017. Geothermal gradient, Curie point depth and heat flow determination of some parts of lower Benue trough and Anambra basin, Nigeria, Using High Resolution Aeromagnetic Data. Physical Science International Journal, 1–11.

Benkhelil, J., 1989. The origin and evolution of the Cretaceous Benue Trough (Nigeria). Journal of African Earth Sciences (and the Middle East) 8, 251–282. https://doi.org/10.1016/S0899-5362(89)80028-4

Beukes, N.J., 1987. Facies relations, depositional environments and diagenesis in a major early Proterozoic stromatolitic carbonate platform to basinal sequence, Campbellrand Subgroup, Transvaal Supergroup, Southern Africa. Sedimentary Geology 54, 1–46.

Bokanda, E.E., Fralick, P., Ekomane, E., Bisse, S.B., Tata, C.N., Ashukem, E.N., Belinga, B.C., 2021. Geochemical constraints on the provenance, paleoweathering and maturity of the Mamfe black shales, West Africa. Journal of African Earth Sciences 175, 104078.

Bolarinwa, A.T., Idakwo, S.O., Bish, D.L., 2019. Rare-earth and trace elements and hydrogen and oxygen isotopic compositions of Cretaceous kaolinitic sediments from the Lower Benue Trough, Nigeria: provenance and paleoclimatic significance. Acta Geochimica 38, 350–363.

Boström, K., 1970. Submarine volcanism as a source for iron. Earth and Planetary Science Letters 9, 348–354.

Burke, K., Whiteman, A.J., 1973. Uplift, rifting and the break-up of Africa. Implications of Continental Drift to the Earth Sciences 2, 735–755.

Chang, H., An, Z., Wu, F., Jin, Z., Liu, W., Song, Y., 2013. A Rb/Sr record of the weathering response to environmental changes in westerly winds across the Tarim Basin in the late Miocene to the early Pleistocene. Palaeogeography, Palaeoclimatology, Palaeoecology 386, 364–373.

Chen, L., Jiang, S., Chen, P., Chen, X., Zhang, B., Zhang, G., Lin, W., Lu, Y., 2021a. Relative sea-level changes and organic matter enrichment in the Upper Ordovician-Lower Silurian Wufeng-Longmaxi Formations in the Central Yangtze area, China. Marine and Petroleum Geology 124, 104809.

Chen, Q., Li, Z., Dong, S., Yu, Q., Zhang, C., Yu, X., 2021b. Applicability of chemical weathering indices of eolian sands from the deserts in northern China. CATENA 198, 105032.

Cheng, Y., Liu, W., Wu, W., Zhang, Y., Tang, G., Liu, C., Nie, Q., Wen, Y., Lu, P., Zhang, C., 2021. Geochemical characteristics of the lower Cambrian Qiongzhusi Formation in Huize area, east Yunnan: implications for paleo-ocean environment and the origin of black rock series. Arabian Journal of Geosciences 14, 1–16.

Chumakov, N.M., Zharkov, M.A., Herman, A.B., Doludenko, M.P., Kalandadze, N.N., Lebedev, E.L., Ponomarenko, A.G., Rautian, A.S., 1995. Climatic belts of the mid-Cretaceous time. Stratigraphy and Geological Correlation 3, 42–63.

Cox, R., Lowe, D.R., Cullers, R.L., 1995. The influence of sediment recycling and basement composition on evolution of mudrock chemistry in the southwestern United States. Geochimica et Cosmochimica Acta 59, 2919–2940.

Dim, C.I.P., Onuoha, K.M., Okwara, I.C., Okonkwo, I.A., Ibemesi, P.O., 2019. Facies analysis and depositional environment of the Campano–Maastrichtian coal-bearing Mamu Formation in the Anambra Basin, Nigeria. Journal of African Earth Sciences 152, 69–83.

Edegbai, A.J., Schwark, L., Oboh-Ikuenobe, F.E., 2020. Nature of dispersed organic matter and paleoxygenation of the Campano-Maastrichtian dark mudstone unit, Benin flank, western Anambra Basin: Implications for Maastrichtian Trans-Saharan seaway paleoceanographic conditions. Journal of African Earth Sciences 162, 103654.

Edegbai, A.J., Schwark, L., Oboh-Ikuenobe, F.E., 2019a. Campano-Maastrichtian paleoenvironment, paleotectonics and sediment provenance of western Anambra Basin, Nigeria: Multi-proxy evidences from the Mamu Formation. Journal of African Earth Sciences 156, 203–239.

Edegbai, A.J., Schwark, L., Oboh-Ikuenobe, F.E., 2019b. A review of the latest Cenomanian to Maastrichtian geological evolution of Nigeria and its stratigraphic and paleogeographic implications. Journal of African Earth Sciences 150, 823–837. https://doi.org/10.1016/j.jafrearsci.2018.10.007

Edegbai and Schwark, 2020. Differentiation of Sediment Source Regions in the Southern Benue Trough and Anambra Basin, Nigeria: Insights from Geochemistry of Upper Cretaceous Strata. Geology, Earth & Marine Sciences 2, 1–37. https://doi.org/10.31038/GEMS.2020224

Ejeh, O.I., 2021. Geochemistry of rocks (Late Cretaceous) in the Anambra Basin, SE Nigeria: insights into provenance, tectonic setting, and other palaeo-conditions. Heliyon 7, e08110.

Elliot, M., Welsh, K., Chilcott, C., McCulloch, M., Chappell, J., Ayling, B., 2009. Profiles of trace elements and stable isotopes derived from giant long-lived *Tridacna gigas* bivalves: potential applications in paleoclimate studies. Palaeogeography, Palaeoclimatology, Palaeoecology 280, 132–142.

Ene, G.E., Okogbue, C.O., Onuoha, K.M., 2019. Evaluating the impact of hydrodynamic flow on the hydrocarbon potentials of the Cretaceous Anambra basin, Southeastern Nigeria. Arabian Journal of Geosciences 12, 644. https://doi.org/10.1007/s12517-019-4810-5

Fairhead, J.D., 1988. Mesozoic plate tectonic reconstructions of the central South Atlantic Ocean: the role of the West and Central African rift system. Tectonophysics 155, 181–191.

Fedo, C.M., Wayne Nesbitt, H., Young, G.M., 1995. Unraveling the effects of potassium metasomatism in sedimentary rocks and paleosols, with implications for paleoweathering conditions and provenance. Geology 23, 921–924.

Fu, X., Wang, J., Chen, W., Feng, X., Wang, D., Song, C., Zeng, S., 2016. Elemental geochemistry of the early Jurassic black shales in the Qiangtang Basin, eastern Tethys: constraints for palaeoenvironment conditions. Geological Journal 51, 443–454.

Gebhardt, H., 1998. Benthic Foraminifera from the Maastrichtian lower Mamu Formation near Leru (southern Nigeria); paleoecology and paleogeographic significance. The Journal of Foraminiferal Research 28, 76–89.

Goldberg, K., Humayun, M., 2016. Geochemical paleoredox indicators in organic-rich shales of the Irati Formation, Permian of the Paraná Basin, southern Brazil. Brazilian Journal of Geology 46, 377–393.

Guo, L., Jiang, Z., Zhang, J., Li, Y., 2011. Paleoenvironment of Lower Silurian black shale and its significance to the potential of shale gas, southeast of Chongqing, China. Energy Exploration & Exploitation 29, 597–616.

Hallberg, R.O., 1976. A geochemical method for investigation of palaeoredox conditions in sediments. Ambio Special Report 4, 139–147.

Han, S., Zhang, Y., Huang, J., Rui, Y., Tang, Z., 2020. Elemental Geochemical Characterization of Sedimentary Conditions and Organic Matter Enrichment for Lower Cambrian Shale Formations in Northern Guizhou, South China. Minerals 10, 793.

Harnois, L., 1988. The CIW index: a new chemical index of weathering. Sedimentary Geology 55, 319–322.

Hatch, J.R., Leventhal, J.S., 1992. Relationship between inferred redox potential of the depositional environment and geochemistry of the Upper Pennsylvanian (Missourian) Stark Shale Member of the Dennis Limestone, Wabaunsee County, Kansas, USA. Chemical Geology 99, 65–82.

Hay, W.W., Floegel, S., 2012. New thoughts about the Cretaceous climate and oceans. Earth-Science Reviews 115, 262–272.

Herron, M.M., 1988. Geochemical classification of terrigenous sands and shales from core or log data. Journal of Sedimentary Research 58, 820–829.

Hu, J., Li, Q., Song, C., Wang, S., Shen, B., 2017. Geochemical characteristics of the Permian sedimentary rocks from Qiangtang Basin: constraints for paleoenvironment and paleoclimate. Terrestrial, Atmospheric and Oceanic Sciences 28, 271–282.

Huang, H., He, D., Li, D., Li, Y., Zhang, W., Chen, J., 2020. Geochemical characteristics of organic-rich shale, Upper Yangtze Basin: Implications for the Late Ordovician–Early

Silurian orogeny in South China. Palaeogeography, Palaeoclimatology, Palaeoecology 554, 109822.

Jones, B., Manning, D.A., 1994. Comparison of geochemical indices used for the interpretation of palaeoredox conditions in ancient mudstones. Chemical Geology 111, 111–129.

Kahmann, J.A., Seaman, J., Driese, S.G., 2008. Evaluating trace elements as paleoclimate indicators: multivariate statistical analysis of late Mississippian Pennington Formation paleosols, Kentucky, USA. The Journal of Geology 116, 254–268.

Kidder, D.L., Erwin, D.H., 2001. Secular distribution of biogenic silica through the Phanerozoic: comparison of silica-replaced fossils and bedded cherts at the series level. The Journal of Geology 109, 509–522.

Kloss, T.J., Dornbos, S.Q., Chen, J.-Y., McHenry, L.J., Marenco, P.J., 2015. High-resolution geochemical evidence for oxic bottom waters in three Cambrian Burgess Shale-type deposits. Palaeogeography, Palaeoclimatology, Palaeoecology 440, 90–95.

Krzeszowska, E., 2019. Geochemistry of the Lublin Formation from the Lublin Coal Basin: Implications for weathering intensity, palaeoclimate and provenance. International Journal of Coal Geology 216, 103306.

Ladant, J.-B., Poulsen, C.J., Fluteau, F., Tabor, C.R., MacLeod, K.G., Martin, E.E., Haynes, S.J., Rostami, M.A., 2020. Paleogeographic controls on the evolution of Late Cretaceous ocean circulation. Climate of the Past 16, 973–1006.

Lai, H., Li, M., Liu, J., Mao, F., Xiao, H., He, W., Yang, L., 2018. Organic geochemical characteristics and depositional models of Upper Cretaceous marine source rocks in the Termit Basin, Niger. Palaeogeography, Palaeoclimatology, Palaeoecology 495, 292–308. https://doi.org/10.1016/j.palaeo.2018.01.024

Leyuan, F., Jiapeng, W., Wan, D., Yang, L.I., 2021. Sedimentary characteristics of the shallow water delta in rifted lacustrine basin: A case study in the Aradeiba Formation, Unity Sag, Muglad Basin. Earth Science Frontiers 28, 155.

Li, D., Li, R., Zhu, Z., Wu, X., Liu, F., Zhao, B., Cheng, J., Wang, B., 2018a. Elemental characteristics and paleoenvironment reconstruction: a case study of the Triassic lacustrine Zhangjiatan oil shale, southern Ordos Basin, China. Acta Geochimica 37, 134–150.

Li, D., Li, R., Zhu, Z., Xu, F., 2018b. Elemental characteristics of lacustrine oil shale and its controlling factors of palaeo-sedimentary environment on oil yield: a case from Chang 7 oil layer of Triassic Yanchang Formation in southern Ordos Basin. Acta Geochimica 37, 228–243.

Li, H., Liu, B., Liu, X., Meng, L., Cheng, L., Wang, H., 2019. Mineralogy and inorganic geochemistry of the Es4 shales of the Damintun Sag, northeast of the Bohai Bay Basin: Implication for depositional environment. Marine and Petroleum Geology 110, 886–900.

Li, T.-J., Huang, Z.-L., Chen, X., Li, X.-N., Liu, J.-T., 2021. Paleoenvironment and organic matter enrichment of the Carboniferous volcanic-related source rocks in the Malang Sag, Santanghu Basin, NW China. Petroleum Science 18, 29–53.

Li, X., Gang, W., Yao, J., Gao, G., Wang, C., Li, J., Liu, Y., Guo, Y., Yang, S., 2020. Major and trace elements as indicators for organic matter enrichment of marine carbonate rocks: A case study of Ordovician subsalt marine formations in the central-eastern Ordos Basin, North China. Marine and Petroleum Geology 111, 461–475.

Liu, Z., Zhao, Y., Colin, C., Siringan, F.P., Wu, Q., 2009. Chemical weathering in Luzon, Philippines from clay mineralogy and major-element geochemistry of river sediments. Applied Geochemistry 24, 2195–2205.

Long, X., Yuan, C., Sun, M., Xiao, W., Wang, Y., Cai, K., Jiang, Y., 2012. Geochemistry and Nd isotopic composition of the Early Paleozoic flysch sequence in the Chinese Altai, Central Asia: evidence for a northward-derived mafic source and insight into Nd model ages in accretionary orogen. Gondwana Research 22, 554–566.

Loubser, M., Verryn, S., 2008. Combining XRF and XRD analyses and sample preparation to solve mineralogical problems. South African Journal of Geology 111, 229–238. https://doi.org/10.2113/gssajg.111.2-3.229

Martinez-Ruiz, F., Kastner, M., Gallego-Torres, D. Rodrigo-Gámiz, M., Nieto-Moreno, V., Ortega-Huertas, M., 2015. Paleoclimate and paleoceanography over the past 20,000 yr in the Mediterranean Sea Basins as indicated by sediment elemental proxies. Quaternary Science Reviews 107, 25–46.

McLennan, S.M., Hemming, S., McDaniel, D.K., Hanson, G.N., 1993. Geochemical approaches to sedimentation, provenance, and tectonics, in: Johnsson, M.J., Basu, A. (Eds.), Processes Controlling the Composition of Clastic Sediments. Geological Society of America, Special Papers 285, pp. 21-40. http://dx.doi.org/10.1130/SPE284-p21.

Miall, A.D., 2006. Reconstructing the architecture and sequence stratigraphy of the preserved fluvial record as a tool for reservoir development: A reality check. AAPG Bulletin 90, 989–1002.

Miall, A.D., 1988. Architectural elements and bounding surfaces in fluvial deposits: anatomy of the Kayenta Formation (Lower Jurassic), southwest Colorado. Sedimentary Geology 55, 233–262.

Miall, A.D., 1977. Lithofacies types and vertical profile models in braided river deposits: a summary. In: Miall, A.D. (ed.) Fluvial Sedimentology. Geological Survey of Canada, Calgary, pp. 597-604.

Mode, A.W., Anyiam, O.A., Anigbogu, E.C., 2016. The effect of diagenesis on reservoir quality of Mamu Sandstone, Anambra Basin, Nigeria. Journal of the Geological Society of India 87, 583–590.

Mode, A.W., Odumodu, C.F.R., 2015. Lithofacies and ichnology of the Late Maastrichtian–Danian Nsukka Formation in the Okigwe area, Anambra Basin, Southeastern Nigeria. Arabian Journal of Geosciences 8, 7455–7466.

Moradi, A.V., Sarı, A., Akkaya, P., 2016. Geochemistry of the Miocene oil shale (Hançili Formation) in the Çankırı-Çorum Basin, Central Turkey: Implications for Paleoclimate conditions, source–area weathering, provenance and tectonic setting. Sedimentary Geology 341, 289–305.

Nath, B.N., Bau, M., Rao, B.R., Rao, C.M., 1997. Trace and rare earth elemental variation in Arabian Sea sediments through a transect across the oxygen minimum zone. Geochimica et Cosmochimica Acta 61, 2375–2388.

Nesbitt, H.W., Young, G.M., 1984. Prediction of some weathering trends of plutonic and volcanic rocks based on thermodynamic and kinetic considerations. Geochimica et Cosmochimica Acta 48, 1523–1534.

Nesbitt, Hw., Young, G.M., 1982. Early Proterozoic climates and plate motions inferred from major element chemistry of lutites. Nature 299, 715–717.

Nwajide, C.S., 1990. Cretaceous sedimentation and paleogeography of the central Benue Trough. The Benue. Tough Structure and Evolution International Monograph Series, Braunschweig 19–38.

Nwajide, C.S., Reijers, T.J.A., 1996. Geology of the southern Anambra Basin. Selected Chapters on Geology, SPDC, Warri 133–148.

Obaje, N.G., 2009. Geology and mineral resources of Nigeria. Springer.

Obasi, A.I., Selemo, A.O.I., Nomeh, J.S., 2018. Gravity models as tool for basin boundary demarcation: A case study of Anambra Basin, Southeastern Nigeria. Journal of Applied Geophysics 156, 31–43.

Oboh-Ikuenobe, F.E., Obi, C.G., Jaramillo, C.A., 2005. Lithofacies, palynofacies, and sequence stratigraphy of Palaeogene strata in Southeastern Nigeria. Journal of African Earth Sciences 41, 79–101. https://doi.org/10.1016/j.jafrearsci.2005.02.002

Ocheli, A., Okoro, A.U., Ogbe, O.B., Aigbadon, G.O., 2018. Granulometric and pebble morphometric applications to Benin Flank sediments in western Anambra Basin, Nigeria: proxies for paleoenvironmental reconstruction. Environmental Monitoring and Assessment 190, 1–17.

Odunze, O.S., Obi, S.G.C., 2011. Sequence stratigraphic framework of the Imo Formation in the Southern Benue Trough. Journal of Mining and Geology 47, 135–146.

Odunze, S.O., Obi, G.C., Yuan, W., Min, L., 2013. Sedimentology and sequence stratigraphy of the Nkporo Group (Campanian–Maastrichtian), Anambra Basin, Nigeria. Journal of Palaeogeography 2, 192–208.

Ogungbesan, G.O., Adedosu, T.A., 2020. Geochemical record for the depositional condition and petroleum potential of the Late Cretaceous Mamu Formation in the western flank of Anambra Basin, Nigeria. Green Energy & Environment 5, 83–96.

Ojo, O.J., Akande, S.O., 2008. Microfloral assemblage, age and paleoenvironment of the upper Cretaceous Patti Formation, southeastern Bida Basin, Nigeria. Journal of Mining and Geology 44, 71–81.

Ojo, O.J., Bamidele, T.E., Adepoju, S.A., Akande, S.O., 2021. Genesis and paleoenvironmental analysis of the ironstone facies of the Maastrichtian Patti Formation, Bida Basin, Nigeria. Journal of African Earth Sciences 174, 104058. https://doi.org/10.1016/j.jafrearsci.2020.104058

Okwara, I.C., Dim, C.I.P., Anyiam, O.A., 2020. Reservoir evaluation within the sequence stratigraphic framework of the Upper Cretaceous Anambra Basin, Nigeria. Journal of African Earth Sciences 162, 103708.

Ola-Buraimo, A.O., Yelwa, N.A., Aliyu, M., 2016. Appraisal of the Middle Cretaceous Sediments in Ubiaja-1 well Through the Use of Palynology in Anambra Basin, Southeastern Nigeria. Current Journal of Applied Science and Technology 1–11.

Omietimi, E.J., Chouhan, A.K., Lenhardt, N., Yang, R., Bumby, A.J., 2021. Structural interpretation of the south-western flank of the Anambra Basin (Nigeria) using satellite-derived WGM 2012 gravity data. Journal of African Earth Sciences, 182, 104290.

Onoduku, U., Okosun, E., Obaje, N., Goro, I., Salihu, H., Chukwuma-Orji, J., 2017. Palynological Evidence of a Campanian-Maastrichtian Age of the Central Bida Basin, Nigeria: Implication for Paleoenvironment, Paleoclimate and Hydrocarbon Prospectivity. Minna Journal of Geosciences 1, 165–178.

Onuigbo, E.N., Etu-Efeotor, J.O., Okoro, A.U., 2012. Palynology, paleoenvironment and sequence stratigraphy of the campanian-maastrichtian deposits in the anambra basin, Southeastern Nigeria. European Journal of Scientific Research 78, 333–348.

Onwuemesi, A.G., 1997. One-dimensional spectral analysis of aeromagnetic anomalies and Curie depth isotherm in the Anambra Basin of Nigeria. Journal of Geodynamics 23, 95–107.

Overare, B., Osokpor, J., Ekeh, P.C., Azmy, K., 2020. Demystifying provenance signatures and paleo-depositional environment of mudrocks in parts of south-eastern Nigeria: Constraints from geochemistry. Journal of African Earth Sciences 172, 103954.

Parker, A., 1970. An index of weathering for silicate rocks. Geological Magazine 107, 501–504.

Pehlivanli, B.Y., 2019. Factors controlling the paleo-sedimentary conditions of Çeltek oil shale, Sorgun-Yozgat/Turkey. Maden Tetkik ve Arama Dergisi 158, 251–263.

Reijers, T.J.A., Petters, S.W., Nwajide, C.S., 1997. Chapter 7 The niger delta basin. In: Selley, R.C. (Ed.), Sedimentary Basins of the World, African Basins. Elsevier, 151–172. https://doi.org/10.1016/S1874-5997(97)80010-X

Rimmer, S.M., 2004. Geochemical paleoredox indicators in Devonian–Mississippian black shales, Central Appalachian Basin (USA). Chemical Geology, Geochemistry of Organic-Rich Shales: New Perspectives 206, 373–391. https://doi.org/10.1016/j.chemgeo.2003.12.029

Rudnick, R.L., Gao, S., 2003. 3.01 - Composition of the Continental Crust. In: Holland, H.D., Turekian, K.K. (Eds.), Treatise on Geochemistry. Pergamon, Oxford, 1–64. https://doi.org/10.1016/B0-08-043751-6/03016-4

Schoenborn, W.A., Fedo, C.M., 2011. Provenance and paleoweathering reconstruction of the Neoproterozoic Johnnie Formation, southeastern California. Chemical Geology 285, 231–255.

Scotese, C.R., Song, H., Mills, B.J., van der Meer, D.G., 2021. Phanerozoic paleotemperatures: The earth's changing climate during the last 540 million years. Earth-Science Reviews, 103503.

Sellwood, B.W., Valdes, P.J., 2006. Mesozoic climates: General circulation models and the rock record. Sedimentary Geology 190, 269–287.

Sprague, R.A., Melvin, J.A., Conradi, F.G., Pearce, T.J., Dix, M.A., Hill, S.D., Canham, H., 2009. Integration of core-based chemostratigraphy and petrography of the Devonian Jauf Sandstones, Uthmaniya area, Ghawar field, eastern Saudi Arabia. Search and Discovery Article 20065, 34.

Takamatsu, T., Kawai, T., Nishikawa, M., 2000. Elemental composition of short sediment cores and ferromanganese concretions from Lake Baikal. Lake Baikal. Elsevier, 155–164.

Tan, M., Zhu, X., Geng, M., Zhu, S., Liu, W., 2017. The occurrence and transformation of lacustrine sediment gravity flow related to depositional variation and paleoclimate in the Lower Cretaceous Prosopis Formation of the Bongor Basin, Chad. Journal of African Earth Sciences 134, 134–148. https://doi.org/10.1016/j.jafrearsci.2017.06.003

Tao, S., Xu, Y., Tang, D., Xu, H., Li, S., Chen, S., Liu, W., Cui, Y., Gou, M., 2017. Geochemistry of the Shitoumei oil shale in the Santanghu Basin, Northwest China: Implications for paleoclimate conditions, weathering, provenance and tectonic setting. International Journal of Coal Geology 184, 42–56.

Taylor, S.R., McLennan, S.M., 1985. The continental crust: its composition and evolution.

Teng, G.E., 2004. The Distribution of elements, carbon and oxygen isotopes on marine strata and environmental correlation between them and hydrocarbon source rocks formation - An example from Ordovician Basin, China. PhD Dissertation. Graduate School of Chinese Academy of Sciences (Lanzhou Institute of Geology), Lanzhou (in Chinese).

Teng, G.E., Liu, W.H., Xu, Y.C., Chen, J.F., 2005. Correlative study on parameters of inorganic geochemistry and hydrocarbon source rocks formative environment. Advances in Earth Sciences 20, 193–200.

Tijani, M.N., Nton, M.E., Kitagawa, R., 2010. Textural and geochemical characteristics of the Ajali Sandstone, Anambra Basin, SE Nigeria: implication for its provenance. Comptes Rendus Geoscience 342, 136–150.

Toyoda, K., 1993. Geochemical history of ancient Lake Biwa in Japan—chemical indicators of sedimentary paleo-environments in a drilled core. Palaeogeography, Palaeoclimatology, Palaeoecology 101, 169–184.

Tribovillard, N., Algeo, T.J., Lyons, T., Riboulleau, A., 2006. Trace metals as paleoredox and paleoproductivity proxies: an update. Chemical Geology 232, 12–32.

Uzoegbu, U.M., Uchebo, U.A., Okafor, I., 2013. Lithostratigraphy of the Maastrictian Nsukka Formation in the Anambra Basin, SE Nigeria. IOSR Journal of Environmental Science, Toxicology, and Food Technology 5, 96–102.

Visser, J.N., Young, G.M., 1990. Major element geochemistry and paleoclimatology of the Permo-Carboniferous glacigene Dwyka Formation and postglacial mudrocks in southern Africa. Palaeogeography, Palaeoclimatology, Palaeoecology 81, 49–57.

Walker, R.G., Cant, D.J., 1984. Sandy fluvial systems. Facies Models 1, 71–89.

Wang, A., Wang, Z., Liu, J., Xu, N., Li, H., 2021. The Sr/Ba ratio response to salinity in clastic sediments of the Yangtze River Delta. Chemical Geology 559, 119923.

Wang, Q., Jiang, F., Ji, H., Jiang, S., Liu, X., Zhao, Z., Wu, Y., Xiong, H., Li, Y., Wang, Z., 2020. Effects of paleosedimentary environment on organic matter enrichment in a saline lacustrine rift basin - A case study of Paleogene source rock in the Dongpu Depression, Bohai Bay Basin. Journal of Petroleum Science and Engineering 195, 107658. https://doi.org/10.1016/j.petrol.2020.107658

Wang, Z., Fu, X., Feng, X., Song, C., Wang, D., Chen, W., Zeng, S., 2017. Geochemical features of the black shales from the Wuyu Basin, southern Tibet: Implications for palaeoenvironment and palaeoclimate. Geological Journal 52, 282–297.

Wei, W., Algeo, T.J., 2020. Elemental proxies for paleosalinity analysis of ancient shales and mudrocks. Geochimica et Cosmochimica Acta 287, 341–366.

Wei, Y., Li, Xiaoyan, Zhang, R., Li, Xiaodong, Lu, S., Qiu, Y., Jiang, T., Gao, Y., Zhao, T., Song, Z., 2021. Influence of a Paleosedimentary Environment on Shale Oil Enrichment: A Case Study on the Shahejie Formation of Raoyang Sag, Bohai Bay Basin, China. Frontiers in Earth Science 9, 736054. https://doi.org/10.3389/feart.2021.736054.

Xi, Z., Tang, S., 2021. Geochemical characteristics and organic matter accumulation of Late Ordovician shale in the Upper Yangtze Platform, South China. Energy Reports 7, 667–682.

Xin, B., Hao, F., Han, W., Xu, Q., Zhang, B., Tian, J., 2021. Paleoenvironment evolution of the lacustrine organic-rich shales in the second member of Kongdian Formation of Cangdong Sag, Bohai Bay Basin, China: Implications for organic matter accumulation. Marine and Petroleum Geology 133, 105244.

Xu, Z., Lu, H., Zhao, C., Wang, X., Su, Z., Wang, Z., Liu, H., Wang, L., Lu, Q., 2011. Composition, origin and weathering process of surface sediment in Kumtagh Desert, Northwest China. Journal of Geographical Sciences 21, 1062–1076.

Yan, C., Jin, Z., Zhao, J., Du, W., Liu, Q., 2018. Influence of sedimentary environment on organic matter enrichment in shale: A case study of the Wufeng and Longmaxi Formations of the Sichuan Basin, China. Marine and Petroleum Geology 92, 880–894.

You, J., Liu, Y., Zhou, D., Zheng, Q., Vasichenko, K., Chen, Z., 2020. Activity of hydrothermal fluid at the bottom of a lake and its influence on the development of high-quality source rocks: Triassic Yanchang Formation, southern Ordos Basin, China. Australian Journal of Earth Sciences 67, 115–128.

Zeng, S., Wang, J., Fu, X., Chen, W., Feng, X., Wang, D., Song, C., Wang, Z., 2015. Geochemical characteristics, redox conditions, and organic matter accumulation of marine oil shale from the Changliang Mountain area, northern Tibet, China. Marine and Petroleum Geology 64, 203–221. https://doi.org/10.1016/j.marpetgeo.2015.02.031

Zhang, K., Liu, R., Liu, Z., Li, L., Wu, X., Zhao, K., 2020. Influence of palaeoclimate and hydrothermal activity on organic matter accumulation in lacustrine black shales from the Lower Cretaceous Bayingebi Formation of the Yin'e Basin, China. Palaeogeography, Palaeoclimatology, Palaeoecology 560, 110007. https://doi.org/10.1016/j. palaeo.2020.11 0007

Zhang, L., Dong, D., Qiu, Z., Wu, C., Zhang, Q., Wang, Y., Liu, D., Deng, Z., Zhou, S., Pan, S., 2021. Sedimentology and geochemistry of Carboniferous-Permian marine-continental transitional shales in the eastern Ordos Basin, North China. Palaeogeography, Palaeoclimatology, Palaeoecology 571, 110389.

Zhang, L., Xiao, D., Lu, Shuangfang, Jiang, S., Lu, Shudong, 2019. Effect of sedimentary environment on the formation of organic-rich marine shale: Insights from major/trace elements and shale composition. International Journal of Coal Geology 204, 34–50.

Zhao, B.S., Li, R.X., Wang, X.Z., Wu, X.Y., Wang, N., Qin, X.L., Cheng, J.H., Li, J.J., 2016. Sedimentary environment and preservation conditions of organic matter analysis of Shanxi formation mud shale in Yanchang exporation area, Ordos Basin. Geological Science and Technology Information 35, 109–117.

Zhong, D.K., Jiang, Z.K., Guo, Q., Sun, H.T., 2015. A review about research history, situation and prospects of hydrothermal sedimentation. Journal of Palaeogeography 17, 285–296.

Figure captions:

Figure 1. (a) Geologic map of Nigeria showing the Anambra Basin (Obaje, 2009); inset: Map of Africa showing the location of Nigeria. (b) Geologic map of the Anambra Basin showing the location of the studied Owan-1 and Ubiaja wells (Nwajide, 1990).

Figure 2. Stratigraphy and depositional environments of the Anambra Basin (Tijani et al., 2010).

Figure 3. Lithostratigraphic section and paleoweathering, paleoclimatic proxies, paleosalinity and primary productivity indicators of the Nkporo, Mamu and Imo formations within the Ubiaja well.

Figure 4. Stratigraphy and paleoredox proxies, hydrodynamic conditions and paleo-water depth of the Nkporo, Mamu and Imo formations within the Ubiaja well.

Figure 5. Lithostratigraphic section and paleoweathering, paleoclimatic proxies, paleosalinity and primary productivity indicators of the Mamu and Imo formations within the Owan-1 well. See Fig. 4 for legend.

Figure 6. Stratigraphy and paleoredox proxies, hydrodynamic conditions and paleo-water depth of the Mamu and Imo formations within the Owan-1 well. See Fig. 4 for legend.

Figure 7. a) Chemical classification of the sampled sedimentary rocks according to Sprague et al. (2009) and (b) according to Herron (1988); c) Biogenic silica concentration in the Nkporo, Mamu and Imo formations (Barbera et al., 2006).

Figure 8. a) Trace element variation diagram with all samples normalized to UCC (Rudnick and Gao, 2003). b) Rare earth elements of all samples normalized to chondrite compositions (Taylor and McLennan, 1985).

Figure 9. (a) Compositional domain of Fe_2O_3 *vs.* K_2O *vs.* Al_2O_3 indicating the distribution of major element oxides in the Nkporo, Mamu and Imo formations (after Overare et al., 2020). (b) The A–CN–K (A=Al_2O_3; CN=(CaO* +Na_2O); K=K_2O) diagram depicts the chemical weathering pattern and sediment recycling (after Xu et al., 2011). (c) The ICV *vs.* CIA plot shows the maturity and severity of chemical weathering (Long et al., 2012). (d) The Th/Sc *vs.* Zr/Sc plot suggests intense sediment recycling and chemically matured rocks (Long et al., 2012).

Declaration of interests

☒The authors declare that they have no known competing financial interests or personal relationships that could have appeared to influence the work reported in this paper.

☐The authors declare the following financial interests/personal relationships which may be considered as potential competing interests:

Highlights

- Intense weathering and high rainfall during the Late Cretaceous in the Anambra Basin
- Brackish to shallow-marine depositional environments
- Geochemical indicators reveal dominantly oxic conditions
- Low primary paleoproductivity was interpreted
- New insights on hydrodynamics and paleowater depth in the Anambra Basin

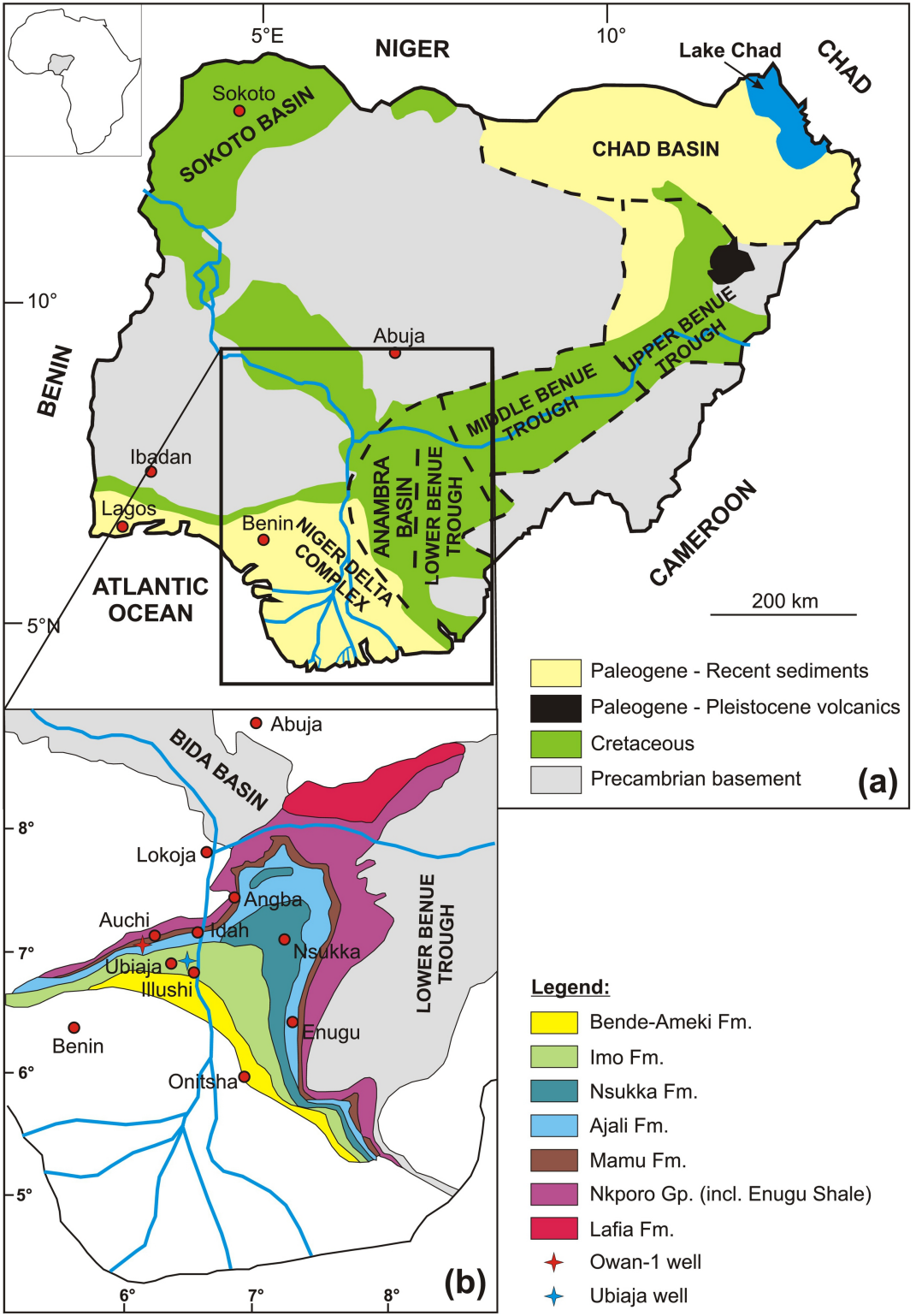
5°E
NIGER
10°
Lake Chad
CHAD
Sokoto
SOKOTO BASIN
CHAD BASIN
10°
BENIN
Abuja
UPPER BENUE TROUGH
MIDDLE BENUE TROUGH
Ibadan
Lagos
Benin
NIGER DELTA COMPLEX
ANAMBRA BASIN
LOWER BENUE TROUGH
CAMEROON
ATLANTIC OCEAN
5°N
200 km
Paleogene - Recent sediments
Paleogene - Pleistocene volcanics
Cretaceous
Precambrian basement
(a)
Abuja
BIDA BASIN
8°
Lokoja
Angba
Auchi
Idah
Nsukka
7°
Ubiaja
Illushi
LOWER BENUE TROUGH
Benin
Enugu
6°
Onitsha
5°
6°
7°
8°
(b)
Legend:
Bende-Ameki Fm.
Imo Fm.
Nsukka Fm.
Ajali Fm.
Mamu Fm.
Nkporo Gp. (incl. Enugu Shale)
Lafia Fm.
Owan-1 well
Ubiaja well

Figure 1

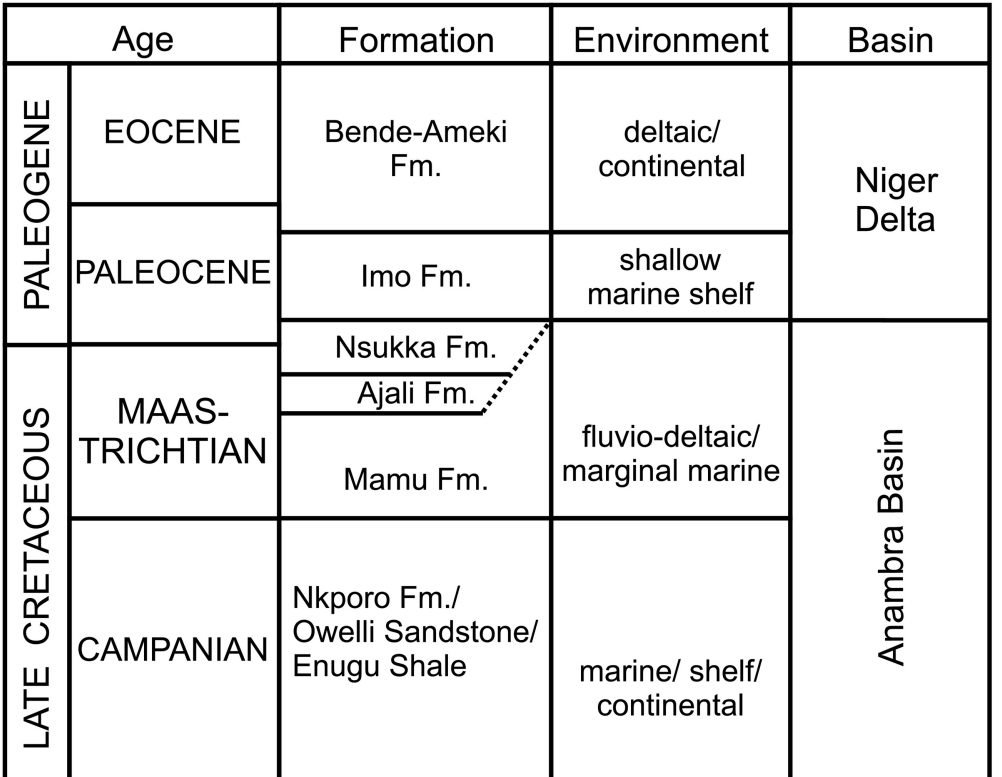
Age
Formation
Environment
Basin
PALEOGENE
EOCENE
PALEOCENE
LATE CRETACEOUS
MAAS-TRICHTIAN
CAMPANIAN
Bende-Ameki Fm.
Imo Fm.
Nsukka Fm.
Ajali Fm.
Mamu Fm.
Nkporo Fm./ Owelli Sandstone/ Enugu Shale
deltaic/ continental
shallow marine shelf
fluvio-deltaic/ marginal marine
marine/ shelf/ continental
Niger Delta
Anambra Basin

Figure 2

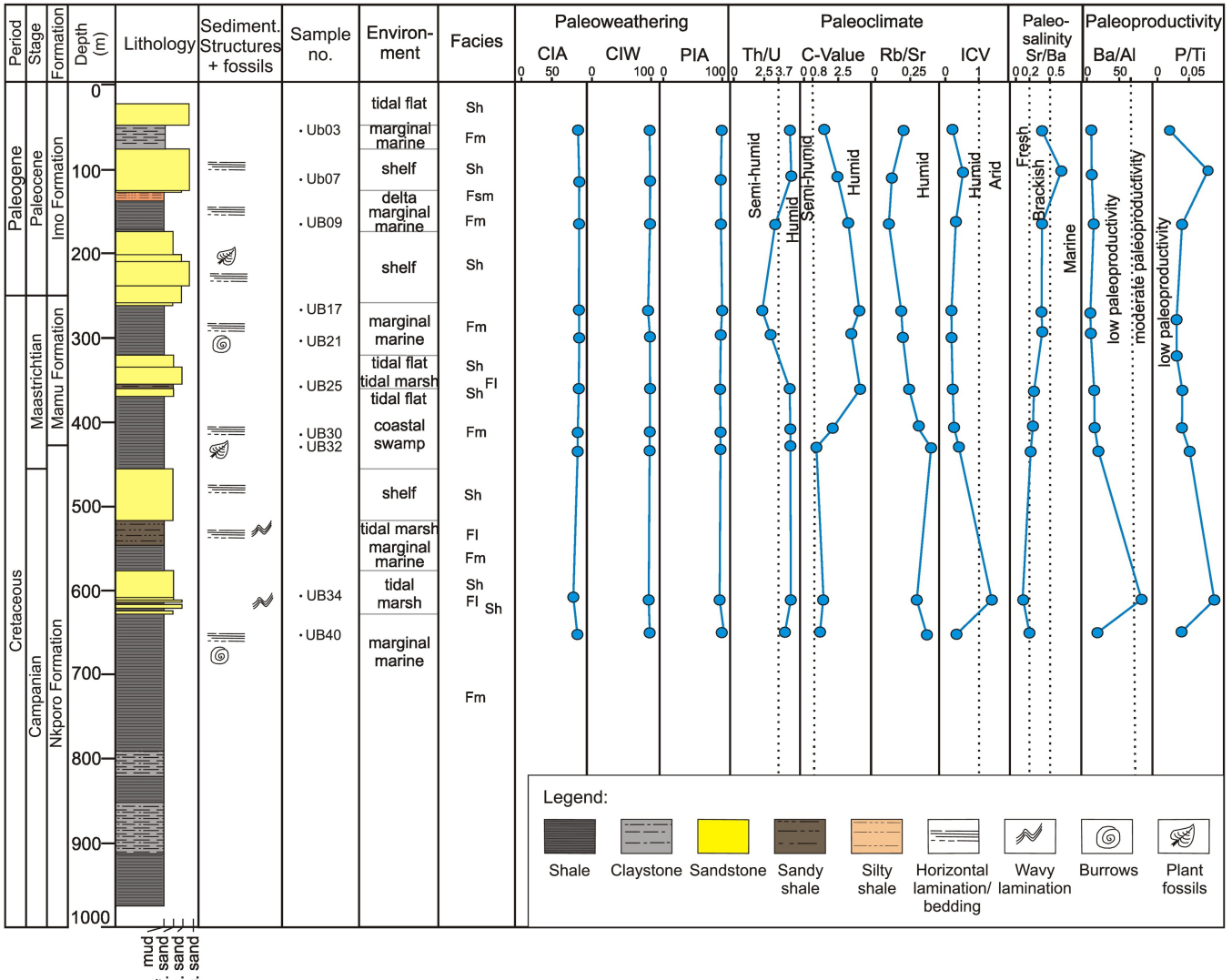
Period
Stage
Formation
Depth (m)
Lithology
Sediment. Structures + fossils
Sample no.
Environ-ment
Facies
Paleoweathering
CIA
CIW
PIA
Paleoclimate
Th/U
C-Value
Rb/Sr
ICV
Paleo-salinity Sr/Ba
Paleoproductivity
Ba/Al
P/Ti
Paleogene
Paleocene
Imo Formation
Cretaceous
Maastrichtian
Mamu Formation
Campanian
Nkporo Formation
tidal flat
marginal marine
shelf
delta
coastal swamp
tidal marsh
Ub03
Ub07
UB09
UB17
UB21
UB25
UB30
UB32
UB34
UB40
Semi-humid
Humid
Arid
Fresh
Brackish
Marine
low paleoproductivity
moderate paleoproductivity
Legend:
Shale
Claystone
Sandstone
Sandy shale
Silty shale
Horizontal lamination/ bedding
Wavy lamination
Burrows
Plant fossils
mud
f. sand
m. sand
c. sand

Figure 3

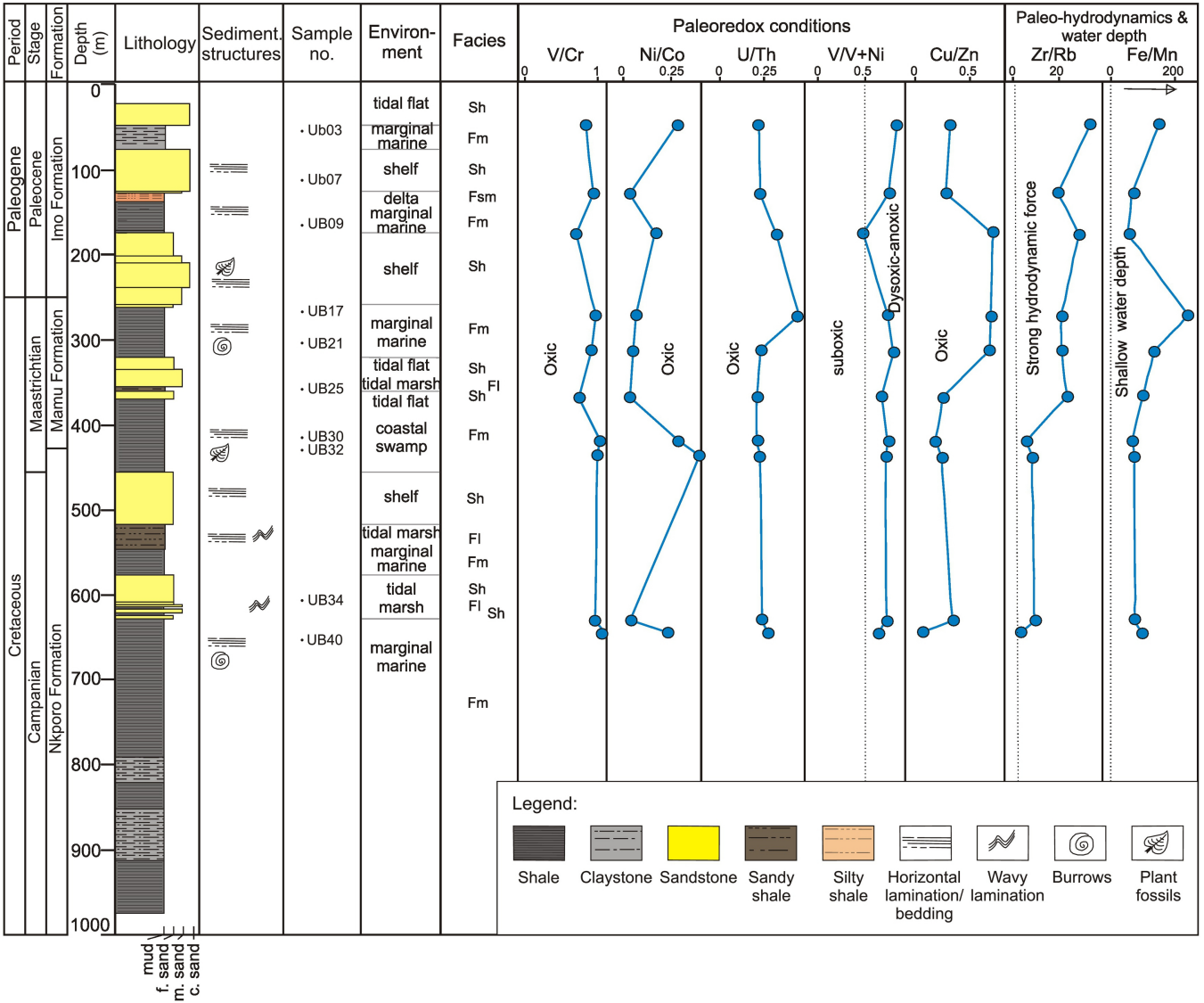
Period
Stage
Formation
Depth (m)
Lithology
Sediment. structures
Sample no.
Environ-ment
Facies
Paleoredox conditions
V/Cr
Ni/Co
U/Th
V/V+Ni
Cu/Zn
Paleo-hydrodynamics & water depth
Zr/Rb
Fe/Mn
Paleogene
Paleocene
Imo Formation
Cretaceous
Maastrichtian
Mamu Formation
Campanian
Nkporo Formation
0
100
200
300
400
500
600
700
800
900
1000
Ub03
Ub07
UB09
UB17
UB21
UB25
UB30
UB32
UB34
UB40
tidal flat
marginal marine
shelf
delta
marginal marine
shelf
marginal marine
tidal flat
tidal marsh
tidal flat
coastal swamp
shelf
tidal marsh
marginal marine
tidal marsh
marginal marine
Sh
Fm
Sh
Fsm
Fm
Sh
Fm
Sh
Fl
Sh
Fm
Sh
Fl
Fm
Sh
Fl
Sh
Fm
Oxic
Oxic
Oxic
suboxic
Dysoxic-anoxic
Oxic
Strong hydrodynamic force
Shallow water depth
mud
f. sand
m. sand
c. sand
Legend:
Shale
Claystone
Sandstone
Sandy shale
Silty shale
Horizontal lamination/ bedding
Wavy lamination
Burrows
Plant fossils

Figure 4

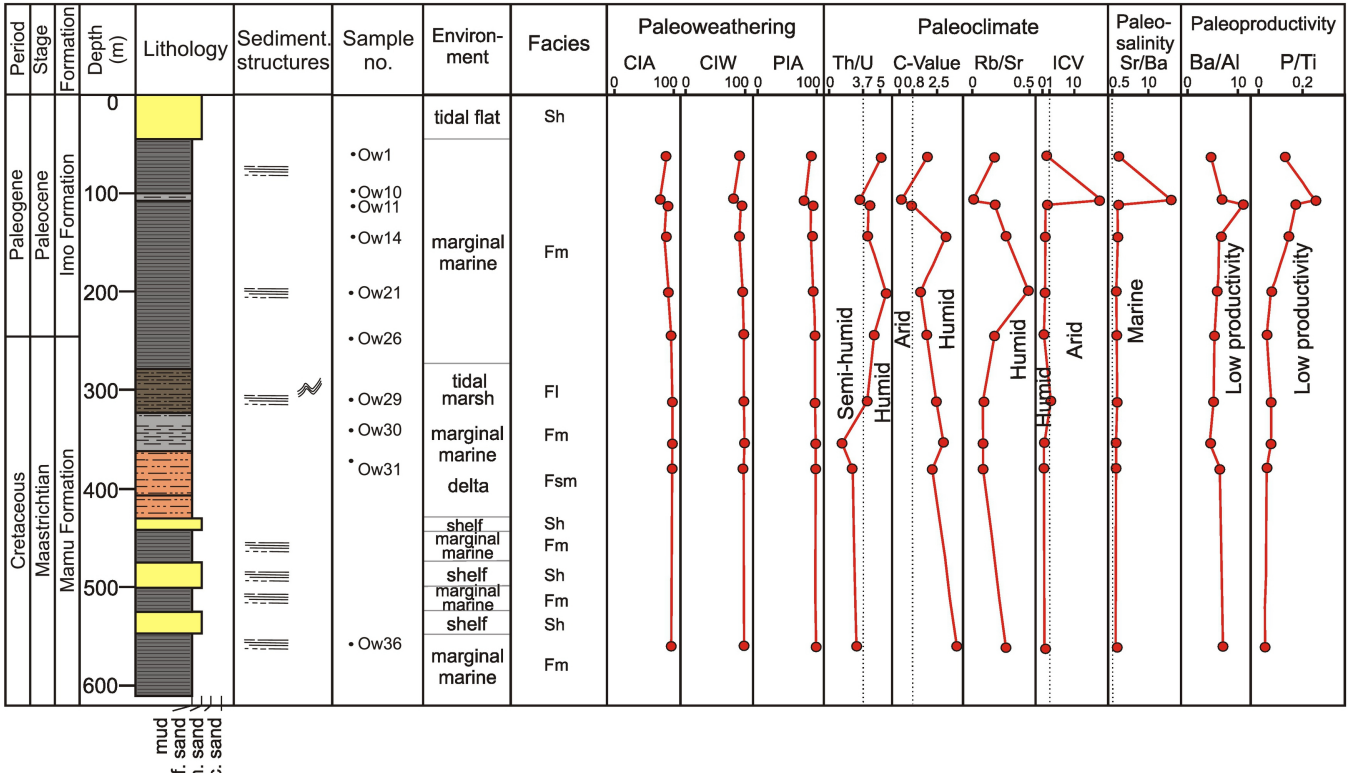
Period
Stage
Formation
Depth (m)
Lithology
Sediment. structures
Sample no.
Environ-ment
Facies
Paleoweathering
CIA
CIW
PIA
Paleoclimate
Th/U
C-Value
Rb/Sr
ICV
Paleo-salinity
Sr/Ba
Paleoproductivity
Ba/Al
P/Ti
Paleogene
Paleocene
Imo Formation
Cretaceous
Maastrichtian
Mamu Formation
0
100
200
300
400
500
600
Ow1
Ow10
Ow11
Ow14
Ow21
Ow26
Ow29
Ow30
Ow31
Ow36
tidal flat
marginal marine
tidal marsh
marginal marine
delta
shelf
marginal marine
shelf
marginal marine
shelf
marginal marine
Sh
Fm
Fl
Fm
Fsm
Sh
Fm
Sh
Fm
Sh
Fm
Semi-humid
Humid
Arid
Humid
Humid
Humid
Arid
Marine
Low productivity
Low productivity
mud
f. sand
m. sand
c. sand

Figure 5

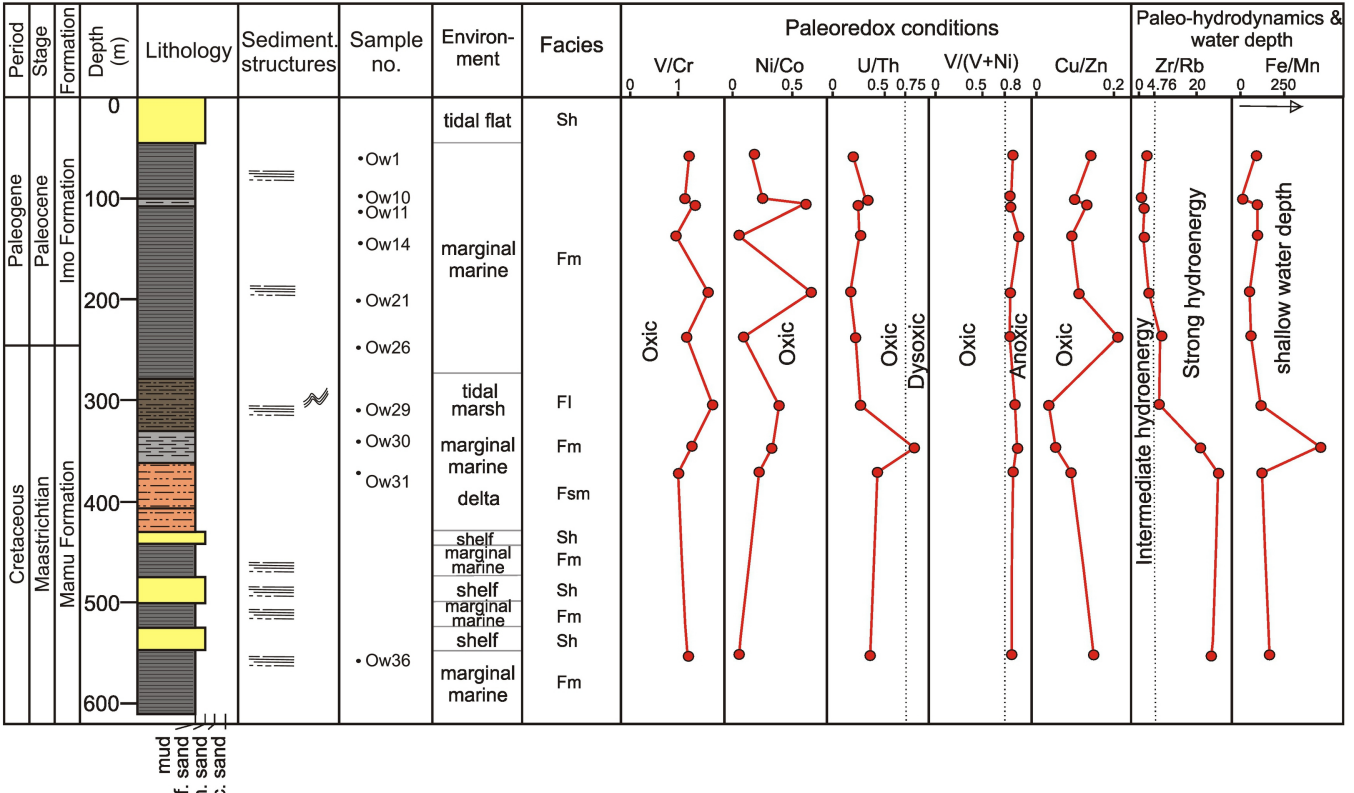
Period
Stage
Formation
Depth (m)
Lithology
Sediment. structures
Sample no.
Environ-ment
Facies
Paleoredox conditions
V/Cr
Ni/Co
U/Th
V/(V+Ni)
Cu/Zn
Paleo-hydrodynamics & water depth
Zr/Rb
Fe/Mn
Paleogene
Paleocene
Imo Formation
Cretaceous
Maastrichtian
Mamu Formation
0
100
200
300
400
500
600
Ow1
Ow10
Ow11
Ow14
Ow21
Ow26
Ow29
Ow30
Ow31
Ow36
tidal flat
marginal marine
tidal marsh
delta
shelf
marginal marine
Sh
Fm
Fl
Fsm
Oxic
Dysoxic
Anoxic
Intermediate hydroenergy
Strong hydroenergy
shallow water depth
mud
f. sand
m. sand
c. sand

Figure 6

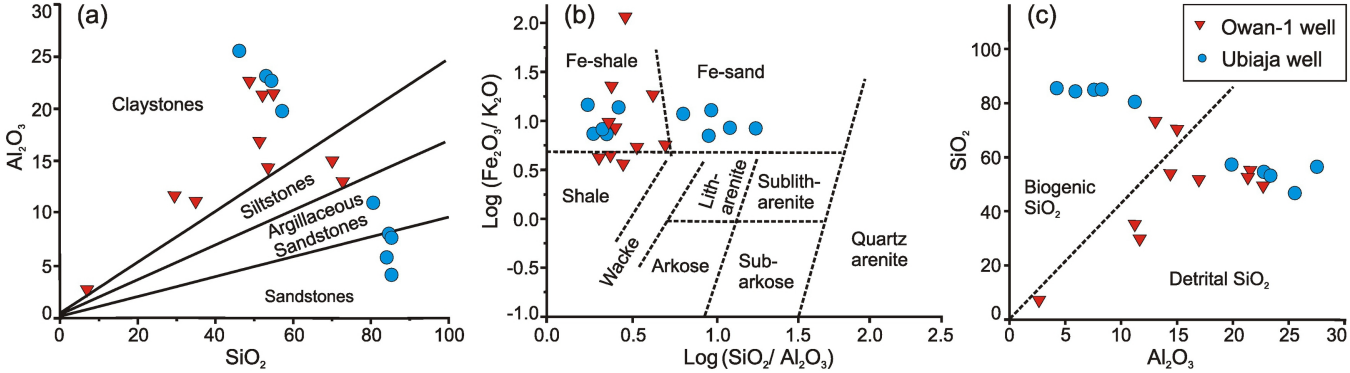
(a)
Claystones
Siltstones
Argillaceous Sandstones
Sandstones
Al_2O_3
SiO_2
(b)
Fe-shale
Fe-sand
Shale
Lith-arenite
Sublith-arenite
Wacke
Arkose
Sub-arkose
Quartz arenite
Log (Fe_2O_3/ K_2O)
Log (SiO_2/ Al_2O_3)
(c)
Owan-1 well
Ubiaja well
Biogenic SiO_2
Detrital SiO_2
SiO_2
Al_2O_3

Figure 7

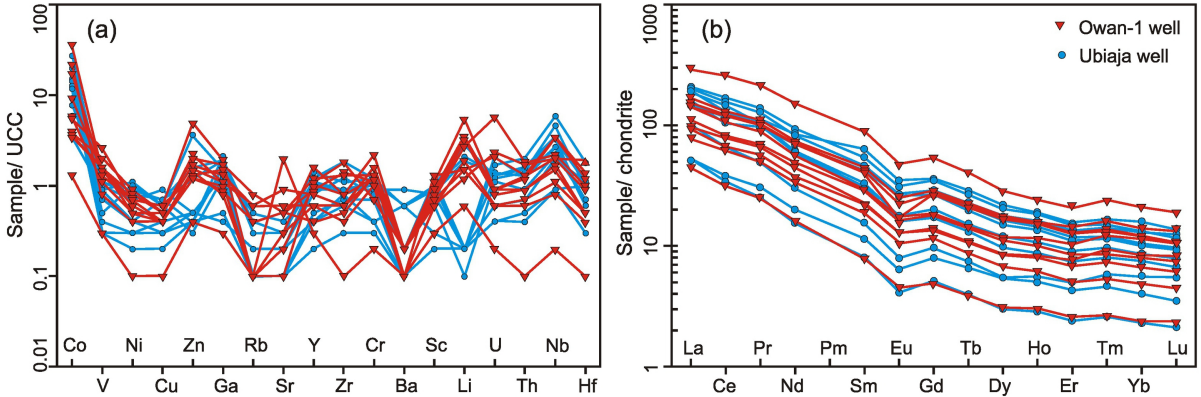
(a)
Sample/ UCC
100
10
1
0.1
0.01
Co
Ni
Zn
Rb
Y
Cr
Sc
U
Nb
V
Cu
Ga
Sr
Zr
Ba
Li
Th
Hf
(b)
Owan-1 well
Ubiaja well
Sample/ chondrite
1000
100
10
1
La
Pr
Pm
Eu
Tb
Ho
Tm
Lu
Ce
Nd
Sm
Gd
Dy
Er
Yb

Figure 8

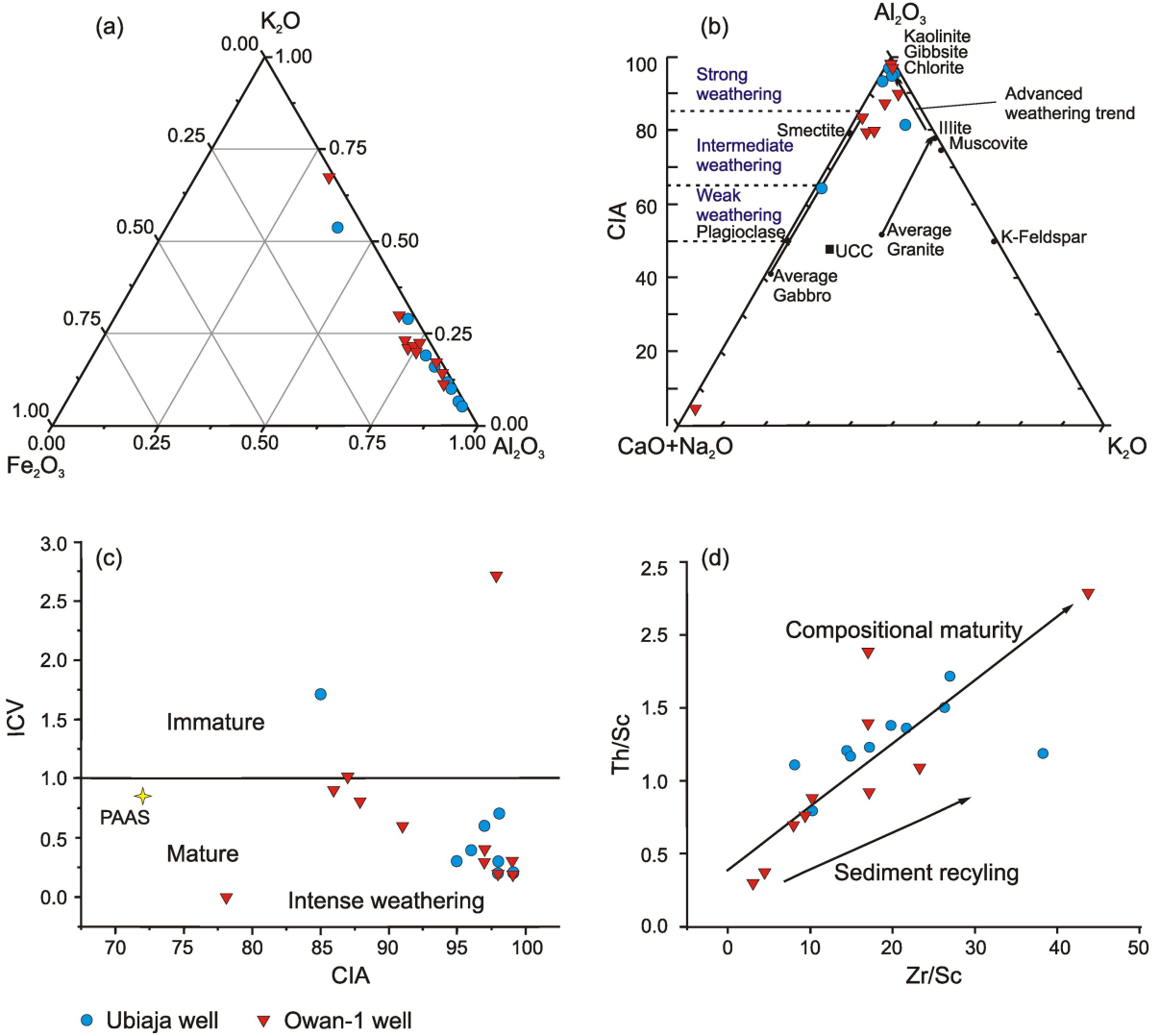
(a)
K_2O
0.00
1.00
0.25
0.75
0.50
0.50
0.75
0.25
1.00
0.00
0.00
0.25
0.50
0.75
1.00
Al_2O_3
Fe_2O_3
(b)
Al_2O_3
Kaolinite
Gibbsite
Chlorite
Strong weathering
Advanced weathering trend
Smectite
Illite
Intermediate weathering
Muscovite
Weak weathering
Plagioclase
Average Granite
K-Feldspar
UCC
Average Gabbro
CIA
100
80
60
40
20
$CaO+Na_2O$
K_2O
(c)
ICV
3.0
2.5
2.0
1.5
1.0
0.5
0.0
Immature
PAAS
Mature
Intense weathering
70
75
80
85
90
95
100
CIA
Ubiaja well
Owan-1 well
(d)
Th/Sc
2.5
2.5
1.5
1.0
0.5
0.0
Compositional maturity
Sediment recyling
0
10
20
30
40
50
Zr/Sc

Figure 9